nature communications

Article

https://doi.org/10.1038/s41467-025-67930-y

Chromatin remodeling factor BAF155 coordinates oligodendroglial-neuronal communications linked to regional myelination and autism-like behavioral deficits in mice

Received: 11 February 2025

Accepted: 12 December 2025

Published online: 21 December 2025

Check for updates

Xiaorui Wang[1], Cong Zeng[2], Zhonghao Wu[1], Minmin Lu[3], Xiao Wang[3], Yun Xiu[4], Qi Wang[1,5], Shouyu Wang[1], Xiaoying Chen[1], Yan Shen[1], Hui Li[1,5], Yixun Su[1,5], Penghui Chen[6], Hui Chen[7], Nengyin Sheng[8], Wei Mo[9,10], Chenju Yi[5], Qingwu Yang[11], Alexei Verkhratsky[12,13,14,15,16], Jianqin Niu[1,2,17,18] ✉ & Lan Xiao[1,19] ✉

Autism spectrum disorders (ASD) are neurodevelopmental disorders associated with synaptic deficits. Oligodendrocyte precursor cells (OPCs) are the only type of glial cells that establish direct synaptic connections with neurons within the central nervous system (CNS). However, the mechanism that results in the delicate construction of OPC-neuron synaptic connections remain poorly understood. Here we show in a mouse model that BAF155, a chromatin remodeling factor, is highly expressed in committed OPCs. BAF155 influences the OPC differentiation and myelination by coordinating the expression of multiple synapse-related genes that mediate OPC-neuron synaptic communication. The varying chromatin regulatory roles of BAF155 across brain regions give rise to local myelin deficits, contributing to the diverse clinical manifestations observed in individuals with ASD. Collectively, these results deepen our insight into OPC-neuron interactions under pathophysiological conditions and uncover a mechanism that integrates synaptic and ASD susceptibility genes, implying that abnormal OPC-neuron synaptogenesis could be an early instigator of ASD.

Autism spectrum disorders (ASD) is one of the most highly heritable (~80%) neurodevelopmental disorders, affecting ~1% of children worldwide[1]. It is characterized by abnormal development of the brain[2,3], resulting in a wide range of psychiatric and neurological symptomology, generally affecting social interactions, and showing restricted and repetitive behaviors[4,5]. At present, the synaptic defect theory is considered the most comprehensive framework in ASD research, as it directly links impaired neuronal connections with excitatory/inhibitory (E/I) imbalances[2,6–12]; however, the underlying pathogenetic mechanisms remain largely obscure.

Recent studies have expanded the understanding of oligodendrocyte precursor cells (OPCs) by demonstrating their interactions with multiple cell types in the central nervous system (CNS)[13]. In a physiological context of OPC–neuron interaction, OPCs are unique among glial cells as they express multiple synapse-related genes and form direct synaptic connections with neurons[14–16], allowing them to

A full list of affiliations appears at the end of the paper. ✉e-mail: jianqinniu@tmmu.edu.cn; xiaolan35@hotmail.com

receive neuronal inputs, then adjusting their behavior accordingly[17], and even play an active role in synaptic pruning and remodeling[18–20]. In pathological conditions, OPCs impede synaptogenesis in hippocampal neuronal networks associated with schizophrenia[21], and facilitate the release of GABA through synaptic complexes with hippocampal interneurons, thereby contributing to anxiety onset[22]. Nonetheless, the primary molecular mechanism that integrates the expressions of multiple synapse genes in OPCs, resulting in the delicate construction of OPC–neuron synaptic connections in ASD conditions, remains poorly understood.

Hence, as part of our strategy, we investigate the regulation of synaptic connections through the lens of autism susceptibility genes. Recently, BAF155, a scaffolding subunit of the BRG1/BRM-associated factor (BAF) complex, was identified as a core member of the SWI/SNF ATP-dependent chromatin remodeling system[23], playing a crucial role in gene expression during embryonic corticogenesis[24–26], and has also been linked to ASD[27–30]. However, it is still largely unknown whether the *Baf155* gene (also known as *Smarcc1* in mice) influences the synaptic communication between OPC and neuron, and how it may contribute to behavioral abnormalities in diseases.

In the current study, we generated a transgenic mouse strain by removing the BAF155 exon 4 from neural stem cells, and found that this caused robust hypomyelination. We used this loxP transgenic mouse to create the conditional knockout of *Baf155* specifically in oligodendroglia, which reproduced multiple autistic behaviors. We provide mechanistic insight into how BAF155 instructs myelination in different brain regions by modifying OPC–neuron communications. Our findings identify an essential chromatin remodeling factor driving OPC–neuron synaptic interactions, and reveal mechanisms of diverse manifestations of ASD, thus highlighting oligodendroglia-oriented interventions as a potential therapeutic strategy.

Results

BAF155 in the CNS regulates oligodendroglial differentiation and myelination

Baf155 mRNA is highly expressed in various cell types in the CNS, including neurons and OPCs, as illustrated in the UMAP plot from the mouse whole-brain transcriptomic cell type atlas[31] (Fig. S1A). To explore the function of *Baf155*, we generated a $Baf155^{fl/fl}$ transgenic mouse, in which the loxP fragments were inserted into the introns downstream of the ATG-containing exon (Fig. S1B). By crossing with $Nestin^{Cre}$ mice, *Baf155* exon 4 was conditionally deleted, which led to a protein reading frame shift in neural stem cells. In this mouse strain, the fl/fl homozygotes were lethal. In order to modify neural cells in a more controlled way, we crossed the $Baf155^{fl/fl}$ transgenic mice with $Nestin^{CreERT2}$ mice, thereby reducing BAF155 protein levels in neural stem cell-derived neurons, astrocytes, and oligodendroglia, but not in microglia (Fig. S1C, S1D). These fl/+ heterozygotes exhibited significant defects in white matter development, as reflected by the reduced myelin-basic protein (MBP)-positive areas (representing the myelin-like structures) (Fig. S1E), along with decreased densities and proportions of PDGFRα-positive OPCs and CC1-positive mature oligodendrocytes (OLs) in medial prefrontal cortex (mPFC); conversely, the ratio of $InsP_3R$-type II (IP_3R-II)/OLIG2-positive committed OPCs was significantly increased (Fig. S1F), indicating a block in the transition from committed OPCs to mature OLs. In addition, other glial cell types and neurons were unaffected (Fig. S1G, S1H). Therefore, our results suggest a major role of BAF155 in the oligodendroglial lineage.

We then explored the expression of BAF155 in oligodendroglia at different developmental stages. A *Pdgfrα-EGFP* mouse strain[32] was employed to identify PDGFRα-expressing OPCs and track OPC differentiation. In addition, the IP_3R-II antibody was used to label committed OPCs[33], whereas CC1 was used to identify differentiated OLs. This multiple staining showed that BAF155 was significantly upregulated in IP_3R-II and PDGFRα-EGFP double-positive committed OPCs, compared to PDGFRα-EGFP-positive but IP_3R-II-negative non-committed OPCs at an earlier developmental stage. Additionally, BAF155 was significantly downregulated in CC1-positive IP_3R-II-negative mature OLs (Fig. 1A). This expression pattern was confirmed in vitro. qPCR conducted on purified OPC cultures revealed that the highest level of *Baf155* mRNA was detected in the committed OPCs (1 day in mitogen-free medium, which switch OPCs to their committed stage), as reflected by the parallel expression of *Gpr17* (indicated by the red dotted line), which has also been reported to be highly expressed in the committed OPCs[34] (Fig. 1B).

To investigate the role of BAF155 in OPC development, $Baf155^{fl/fl}$ transgenic mice were crossed with the OPC-specific $Pdgfr\alpha^{CreER}$ mice (Fig. S2A), allowing *Baf155* knockout before the early differentiation stage at postnatal day 4 (P4, Fig. S2B, S2C). The loss of BAF155 in OPCs resulted in long-lasting defects of oligodendroglial differentiation and myelination, as shown by the reduced numbers of CC1/myelin-associated glycoprotein (MAG)-positive OLs in the mPFC (Fig. S2D, S2E), and persistent decreases of MBP-positive areas in mPFC from P14 to 8-week old (Fig. 1C). Impaired myelination was also confirmed by electron microscopy, showing the reduced number of myelinated axons and increased *G*-ratios (*G*-ratio is defined as the ratio of an axon's diameter to the overall diameter of its myelinated fiber. It serves as an essential metric for evaluating myelin integrity and function; a lower *G*-ratio value reflects thicker myelin sheath and a greater degree of myelination) in *Baf155* knockout mice at both P14 and 8 weeks of age (Fig. 1D, E). Fluorescence microscopy further revealed that the MBP-positive areas on parvalbumin (PV)-positive axons of interneurons, assessed through MBP/PV co-staining, decreased significantly when compared to WT controls. Specifically, there was an 86.86 ± 11.71% reduction at P14, and a 28.68 ± 3.15% reduction at 8 weeks of age (Fig. 1F, G). Loss of BAF155, however, did not affect SMI32-positive axons (Fig. 1F, G), the numbers of OLIG2-positive and PDGFRα-positive oligodendroglial lineage cells (Fig. S2F, S2G), or the proliferation of OPCs (Fig. S2G). These findings indicate that BAF155 predominantly operates during the early oligodendroglial differentiation and myelination.

Loss of BAF155 in committed OPCs induces ASD-like phenotypes

To further determine whether the *Baf155* knockout-induced hypomyelination triggers functional outcomes, we first recorded spontaneous postsynaptic currents in both mPFC (Fig. 2A) and hippocampus (Fig. 2B), both regions being implicated in ASD[2]. Our results showed that loss of BAF155 in OPCs resulted in a significant decrease in the frequency of spontaneous excitatory postsynaptic currents (sEPSC), as well as spontaneous inhibitory postsynaptic currents (sIPSC) in pyramidal neurons in the mPFC and hippocampal CA1 region. In contrast, the amplitudes of postsynaptic currents were unaffected (Fig. 2A, B). Additionally, we recorded miniature synaptic events in the same regions and found that the frequency and amplitude of mEPSCs and mIPSCs remained unchanged in BAF155 knockout mice (Fig. 2C, D). The absence of differences in mEPSC frequency and amplitude suggests that synaptic density appears to be intact; while the action potential-dependent transmission seems to be affected, as indicated by the sEPSC data, which suggests that myelination deficits impair action potential-dependent synaptic transmission.

To investigate which type(s) of behavioral defect is triggered by the loss of BAF155 in OPCs, we first performed the three-chamber test and the self-grooming test, both of which are key behavioral tests associated with ASD. In the first phase of the three-chamber test (social preference test), *Baf155* knockout mice showed a reduced proportion of sniffing time with the chamber containing another mouse (representing the social stimulus) compared to the empty chamber (representing the non-social stimulus). However, in the second phase of the three-chamber test (social novelty preference test), we found no significant difference in the proportion of sniffing time towards the

https://doi.org/10.1038/s41467-025-67930-y

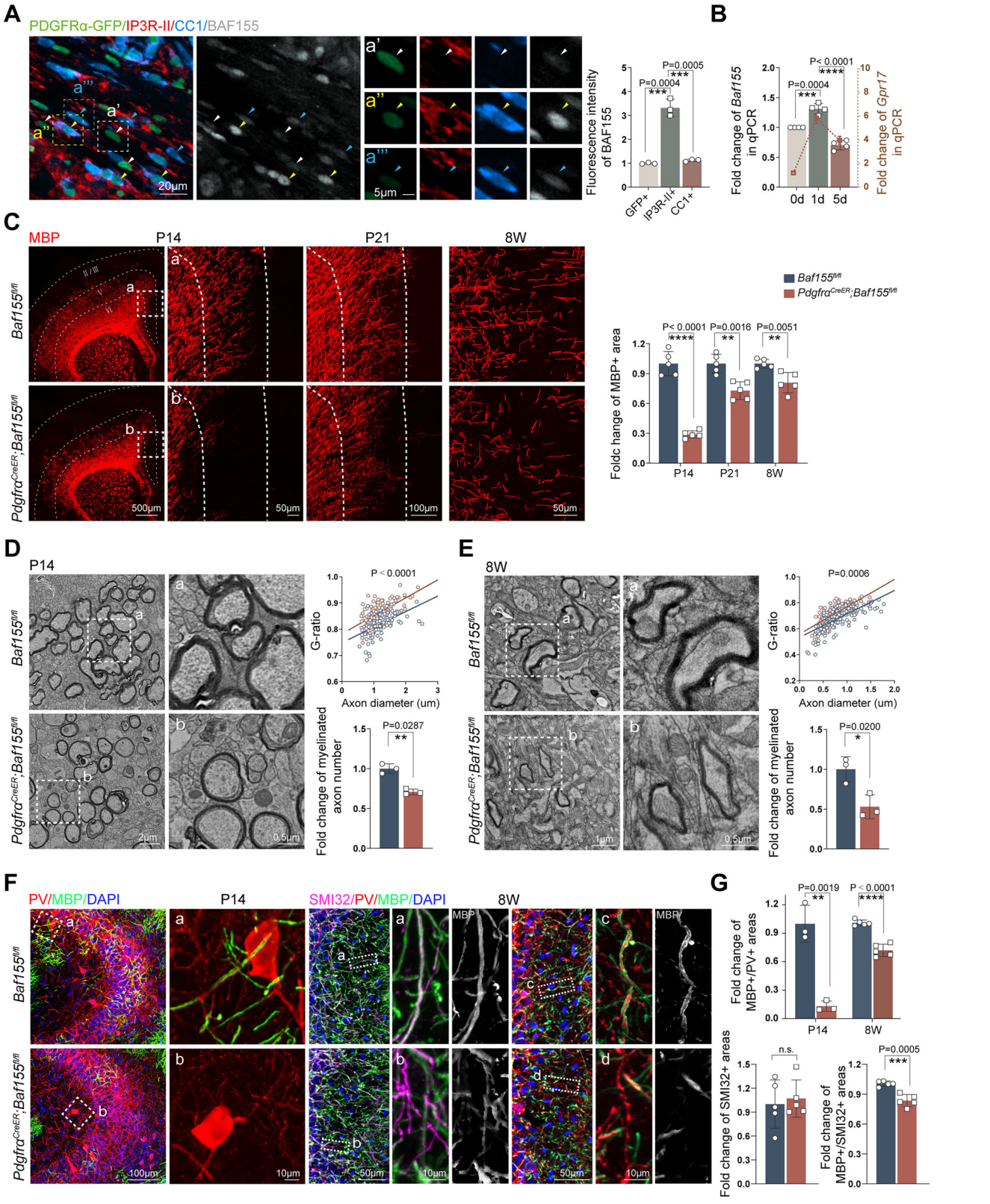

chamber with a stranger mouse (representing the novel social stimulus) versus a familiar mouse (representing the familiar social stimulus) (Fig. 2E). Thus, ASD-like social preference in *Baf155* knockout mice was significantly impaired. In the self-grooming test, *Baf155* knockout mice displayed an increase in repetitive behaviors, suggesting ASD-like restricted and stereotyped movements (Fig. 2F). Subsequently, we performed several cognitive and mental-related behavioral tests. The novel object recognition test showed no differences, suggesting that the loss of BAF155 in OPCs does not affect the memory abilities (Fig. 2G). In the open field test, knockout mice covered less distance in the center of the open field chamber, although there was no difference in the total distance covered (Fig. 2H). In the elevated plus maze test, knockout mice displayed a decrease in the distance traveled in the open arms (Fig. 2I). These changes imply an anxiety-related behavior,

Fig. 1 | BAF155 regulates oligodendroglial differentiation and myelination. **A** Representative image of *Pdgfrα-EGFP* mouse brain stained with IP3R-II, CC1, and BAF155 at P14 and quantification of BAF155 staining in GFP+, IP3R-II+, and CC1+ cells (white arrowheads, OPCs; yellow arrowheads, "committed OPCs"; blue arrowheads, mature Ols). Scale bar = 20 μm, $n = 3$ mice. **B** mRNA expressions of *Baf155* and *Gpr17* (red dotted line) in isolated OPCs at 0, 1, and 5 days after differentiation in vitro, $n = 4$ biological replicates in *Baf155*; $n = 3$ biological replicates in *Gpr17*. **C** Representative images and quantification of MBP staining in the mPFC at P14, P21, and 8 W (scale bar = 500, 100, 50 μm, respectively), $n = 5$ mice. **D** Electron microscopy image of the corpus callosum and quantification of myelinated axon number and *G*-ratio at P14. Scale bar = 2 μm, $n = 3$ mice. **E** Electron microscopy image of the mPFC section and quantification of myelinated axon number and *G*-ratio at 8 weeks. Scale bar, 1 μm. $n = 3$ mice. **F** Representative images of MBP and PV staining in the hippocampal CA3 region at P14 and SMI32, PV, and MBP staining in the hippocampal CA3 region at 8 weeks (scale bar = 100, 50 μm). **G** Upper panel: quantification of MBP+ area in the PV+ region at P14 ($n = 3$ mice) and 8 weeks ($n = 5$ mice). Lower panel: quantification of MBP+ area and MBP+ area in the SMI32+ region at 8 weeks, $n = 5$ mice. The significance between the two experimental groups was ascertained using the unpaired *t*-test. All statistical tests were two-tailed. Data presented as mean ± standard error of the mean (SEM); n.s. not significant, $^{*}p < 0.05$, $^{**}p < 0.01$, $^{***}p < 0.001$, $^{****}p < 0.0001$.

which often presents in ASD patients[35]. Finally, there was no difference in the forced swimming test and tail suspension test between knockout and control mice, suggesting an absence of depression-like behaviors (Fig. 2J, K).

Thus, specific elimination of BAF155 from committed OPCs reproduces several pathophysiological changes seen in ASD, encompassing alterations in neuronal activity and a spectrum of behavioral outcomes.

Loss of BAF155 impairs OPC differentiation and myelin formation

To further investigate the role of BAF155 in regulating oligodendroglial differentiation and myelination, we assessed the characteristics of hypomyelination across various brain regions related to ASD-like behavioral outcomes, as well as in different experimental settings. As shown in our results, the loss of BAF155 in OPCs caused varying reductions of MBP-positive areas across ASD-related brain regions, including mPFC, hippocampus, corpus callosum, cerebellum, and striatum (Figs. 3A, S3A, S3E). Notably, the mPFC exhibited the most significant impact (Figs. 3A, S3A, S3E). To determine whether the reductions in MBP staining are caused by a loss of oligodendroglial lineage cells or by impaired differentiation of OPCs, we also evaluated the staining of CC1, OLIG2, and PDGFRα in various brain regions (Fig. S3B–H) and showed a significant reduction in CC1-positive mature OLs, but no differences in OLIG2+ or PDGFRα+ cells (Fig. S3B–H), suggesting that *Baf155* knockout impairs the OPC differentiation and myelination.

Remyelination is thought to resemble developmental myelination[36], though some studies have found exceptions to this recapitulation hypothesis[37,38]. To investigate the role of BAF155 in remyelination, we employed a model of lysolecithin-induced demyelination in adult mice (Fig. S4A). In this model, the loss of BAF155 did not impact the number of OLIG2-positive oligodendroglial lineage cells within the demyelinating lesions. However, it significantly impaired the differentiation of OPCs, as evidenced by the reduced number of MAG-positive OLs (Figs. 3B and S4B), and it further hindered the remyelination of axons at 14 days post-lesion (Fig. 3C).

To determine whether BAF155 also operates in the OLs, we crossed *Baf155*$^{fl/fl}$ mice with mature OL-specific *Plp*^{CreERT} mice to specifically delete BAF155 at the late stage of OPC differentiation (Fig. S4C). Expression of MBP, numbers of OLIG2-positive oligodendroglial lineage cells, and CC1/MAG-positive mature OLs were unchanged (Figs. 3D, E, S4C, and S4D), demonstrating that depleting BAF155 in OLs does not induce obvious defects in oligodendroglial differentiation and myelination, and providing further confirmation that *Baf155* acts only during early oligodendroglial development, significantly impacting OPC differentiation and myelination.

Intriguingly, when we compared the differentiation capacities of primary OPCs isolated from the cortex of both wild-type and *Baf155* knockout mice, we found that these OPCs showed no difference in their ability to differentiate into MBP-expressing OLs in culture conditions (Fig. 3F). It implies a non-cell autonomous effect involved in BAF155-mediated oligodendroglial development.

Together, these findings raise important questions about the underlying mechanisms through which (1) BAF155 regulates oligodendroglial development in vivo but not in vitro and (2) BAF155 regulates myelination in specific brain regions.

BAF155 targets multiple synaptic genes in committed OPCs

To investigate the underlying mechanism of BAF155 regulating OPC development, we performed chromatin immunoprecipitation sequencing (ChIP-seq) analysis of purified committed OPCs in vitro to identify the potential chromatin remodeling-targeted genes that may trigger autistic symptoms. Our results identified 5226-binding sites of BAF155 located within 3219 genes during the early developmental stage (1 day in mitogen-free medium, which switch OPCs to their committed stage; see Fig. 2B). At the late developmental stage, which corresponds to 5 days in mitogen-free medium, we identified 3810 binding sites located within 2857 genes (Fig. 4A). Among these genes, 928 genes appeared in both early and late developmental stages (Fig. 4A), and the higher BAF155-binding peaks were localized around the transcription start sites (TSS) (Fig. 4B). In addition, most of these binding peaks were found in evolutionarily conserved intergenic regions or introns (Fig. 4C), suggesting that BAF155 mainly targets regulatory regions within the oligodendroglial lineage. Closer examination of these genes and gene ontology (GO) enrichment analysis revealed enrichment in synapse-related genes, including both presynaptic and postsynaptic compartments, but not in myelin-related genes. This enrichment was particularly significant at the early developmental stage (Fig. 4D). Supporting evidence consistently indicated a marked decrease in synapse-related genes during the late developmental stage when compared to the genes that were enriched in the early developmental stage (Fig. 4E). Thus, binding of BAF155 to synapse-associated genes is more pronounced during the early OPC differentiation.

Moreover, we performed a cross-analysis with previously reported ASD susceptibility genes[39–43]. Our results revealed that a substantial number (198 genes) of BAF155-binding genes are synapse-associated, including γ-aminobutyric acid type A receptor subunit γ3 (*Gabrg3* is a member of the GABA-A receptor gene), as well as *Gabrg2*, *Gria2*, *Grm7*, and *Grik2*, which encode subunits of neurotransmitter receptors. Additionally, 17 of these BAF155-binding genes were previously implicated as ASD susceptibility genes, and three of them, including *Gabrg3*, *Adnp* (activity-dependent neuroprotective protein), and Nuclear factor I A (*Nfia*), were identified as both synapse-associated and ASD susceptibility genes. Among these genes, *Gabrg3* emerged as the most prominent synapse-associated ASD susceptibility gene targeted by BAF155 (Fig. 4F). Thus, BAF155-targeted synaptic genes in committed OPCs may play an as-yet-undiscovered role in ASD. To further determine this possibility, we evaluated the fold enrichment of BAF155 on these genes. Our results showed that the enrichments of BAF155 on *Gabrg3*, *Nfia* were significantly higher than other candidate synaptic genes *Gria2*, *Grm7*, *Adnp*, *Gabrg2*, and *Grik2*, particularly in the committed OPC stage (Fig. 4G). In addition, significant enrichments of BAF155 on *Gabrg3* and *Nfia* gene were also detected when compared to the input group in the genome browser visualization, and it is notable

https://doi.org/10.1038/s41467-025-67930-y

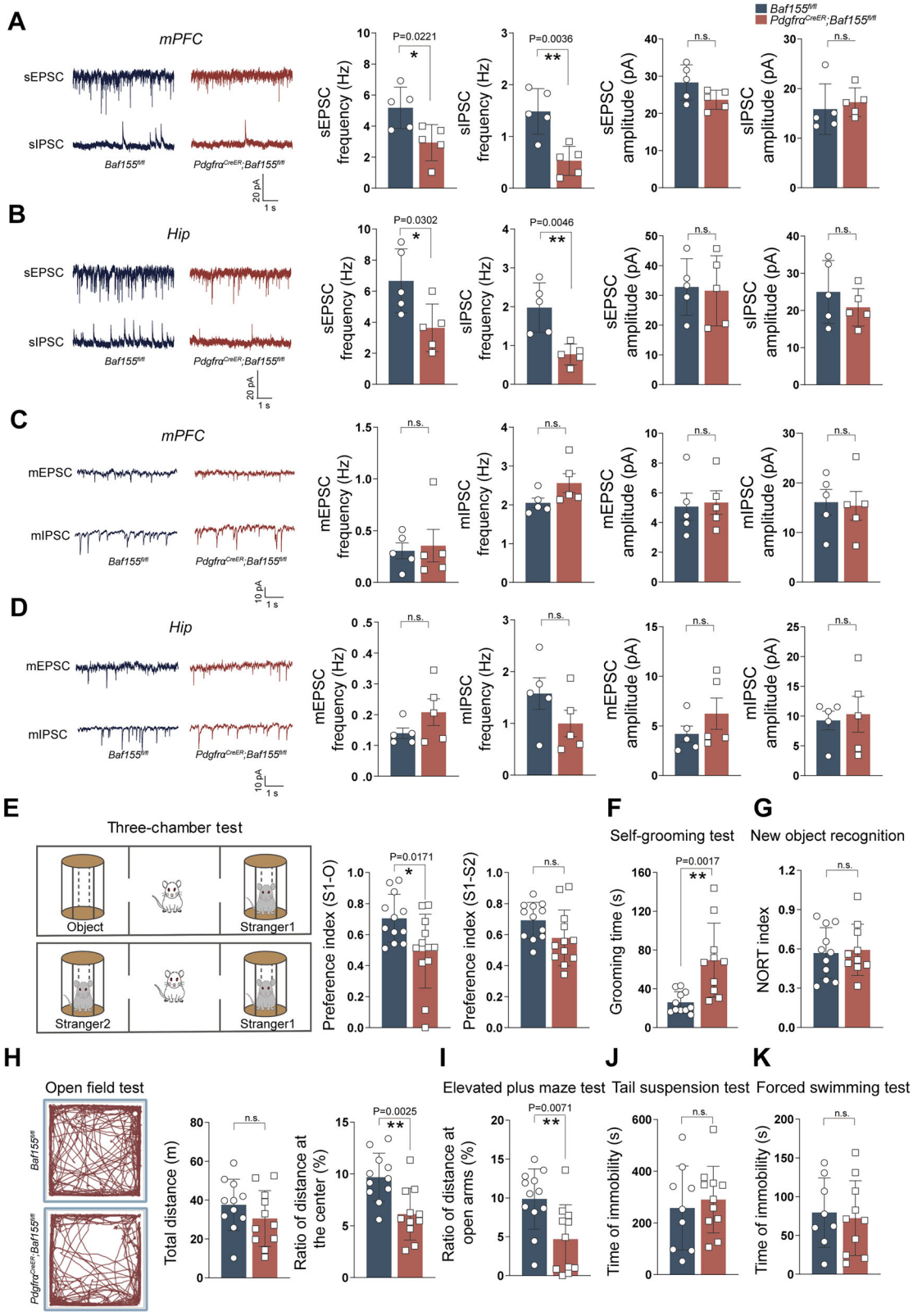

that binding sites of BAF155 on *Gabrg3* and *Nfia* genes were also enriched for H3K27Ac (Histone H3 Lysine 27 acetylation, locates at promoters and enhancers and is strongly correlated with active transcription) but not H3K4me3 (Histone H3 Lysine 4 trimethylation, locates around TSS of active genes)[44–46], again suggesting that BAF155 may target enhancer regions to modulate gene expressions (Fig. 4H, Supplementary Data 1). ChIP-qPCR analysis confirmed significantly increased enrichments of BAF155 protein on *Gabrg3* and *Nfia* genes (Fig. 4I).

These findings indicate that BAF155 predominantly functions during early oligodendroglial development by selectively binding to synaptic genes. This process may be involved in the establishment of OPC–neuron synaptic connections. Since these OPC–neuron synaptic connections are crucial for OPC differentiation and myelination in the

Fig. 2 | Loss of BAF155 in committed OPCs induces ASD-like phenotypes. A and **B** Representative sEPSCs and sIPSCs recordings of the mPFC and hippocampal slices from P21 *Pdgfrα*^{CreER};*Baf155*$^{fl/fl}$ and control mice and quantification of the frequencies and amplitudes, $n = 5$ neurons. **C** and **D** Representative mEPSCs and mIPSCs recordings of the mPFC and hippocampal slices from P21 *Pdgfrα*^{CreER};*Baf155*$^{fl/fl}$ and control mice and quantification of the frequencies and amplitudes, $n = 5$ neurons. **E** The movement patterns and quantification of the three-chamber test in *Pdgfrα*^{CreER};*Baf155*$^{fl/fl}$ and control mice at 6–8 weeks, $n = 12$ mice in *Pdgfrα*^{CreER};*Baf155*$^{fl/fl}$; $n = 12$ mice in control. **F** Quantification of the grooming time in the self-grooming test, $n = 10$ mice in *Pdgfrα*^{CreER};*Baf155*$^{fl/fl}$; $n = 11$ mice in control. **G** Quantification of the novel object recognition test, $n = 10$ mice in *Pdgfrα*^{CreER};*Baf155*$^{fl/fl}$; $n = 11$ mice in control. **H** Representative traces, the total distance, and the ratio of distance traveled in the center during the open field test, $n = 11$ mice in *Pdgfrα*^{CreER};*Baf155*$^{fl/f}$; $n = 11$ mice in control. **I** Quantification of the ratio of distance traveled in the open arms during the elevated plus maze test, $n = 11$ mice in *Pdgfrα*^{CreER};*Baf155*$^{fl/f}$; $n = 12$ mice in control. **J** The immobile time of *Pdgfrα*^{CreER};*Baf155*$^{fl/fl}$ and control mice during the tail suspension test, $n = 11$ mice in *Pdgfrα*^{CreER};*Baf155*$^{fl/fl}$; $n = 9$ mice in control. **K** Immobility time(s) of *Pdgfrα*^{CreER};*Baf155*$^{fl/fl}$ and control mice during the forced swimming test, $n = 10$ mice in *Pdgfrα*^{CreER};*Baf155*$^{fl/fl}$; $n = 8$ mice in control. The significance between the two experimental groups was ascertained using the unpaired *t*-test. All statistical tests were two-tailed. Data are presented as mean ± SEM; n.s. not significant, $^{*}p < 0.05$, $^{**}p < 0.01$.

CNS[14,17,47], we propose that the deficits in differentiation and myelination after BAF155 depletion stem from a lack of neuronal signaling inputs to OPCs. In vitro, the absence of neuronal signaling resulted in no significant changes in OPC differentiation or MBP expression.

BAF155 is required for OPC–neuron synaptic connection

To determine the regulatory role of BAF155 in synaptic connections in OPCs, we measured mRNA and protein levels of these ASD and synapse-associated genes in acutely isolated OPCs and tissue slices from *Pdgfrα*^{CreER};*Baf155*$^{fl/fl}$ mouse brains. The qPCR results showed reduced mRNA levels of *Gabrg3* and *Gabrg2*, as well as *Gria2* in OPCs with *Baf155* deletion (Fig. 5A). Specifically, the numbers of GABRG3-labeled synaptic elements on the surface of OPCs were significantly decreased by 30.54 ± 6.55% in the mPFC, as well as in the hippocampus and corpus callosum (Figs. 5B and S5A).

To investigate whether these BAF155-targeted synaptic genes regulate synaptic connections between OPCs and neurons, the synaptic-like structures on OPCs were examined by super-resolution fluorescence microscopy and immunogold electron microscopy. Both pre- and postsynaptic elements were observed in close association with the OPC cell body and main processes (Figs. 5C, and S5B). We found a significant decrease in postsynaptic elements of OPCs in the brain of *Pdgfrα*^{CreER};*Baf155*$^{fl/fl}$ mice, as reflected by the reduced numbers of Homer1- (an excitatory postsynaptic marker) and Gephyrin- (an inhibitory postsynaptic marker) positive puncta on the PDGFRα-positive OPCs (Figs. 5C, D and S5B). Numbers of vGAT- (a GABAergic presynaptic element marker) and vGLUT1- (a glutamatergic presynaptic marker) positive puncta, closely associated with OPCs, were also significantly declined (Figs. 5C, D and S5B). Furthermore, the immunogold electron microscopy revealed that the length of postsynaptic density in neuron–OPC synapse was significantly reduced by *Baf155* knockout in OPCs (Fig. 5E), confirming that BAF155 regulates OPC–neuron synaptic transmission.

To examine the functionality of OPC–neuron synaptic transmission in *Baf155* deletion mice, we performed calcium imaging in acute brain slices. When monitoring intracellular calcium dynamics in PDGFRα-positive OPCs, we found three distinct patterns of calcium signals in OPCs. As shown by the $\Delta F/F_0$ traces, these three types included: (i) 'flat' Ca^{2+} signaling, (ii) spontaneous 'oscillatory'- Ca^{2+} signaling with peaks, and (iii) spontaneous high 'plateau' transients (Fig. S5C). In *Baf155*-deficient mice, fewer OPCs exhibited oscillatory and plateau patterns; whereas flat Ca^{2+} responses dominated (Figs. 5F and S5D). Moreover, we determined the characteristics of calcium signaling in OPCs. The number of oscillatory peaks per minute was significantly decreased in *Baf155*-deleted OPCs (Fig. 5G and H). We also found that Ca^{2+} transients had greater amplitude in OPCs with *Baf155* deletion (Fig. 5I). This pattern of Ca^{2+} dynamics was documented previously as indicative of oligodendroglial processes that precede retractions from axons[48,49], though the duration of these Ca^{2+} events was comparable to that observed in WT OPCs (Fig. S5D). The number of higher frequencies of Ca^{2+} transients diminished in OPCs lacking BAF155 (Fig. 5J). This specific pattern of Ca^{2+} transients is suggested to play a role in the rapid myelin growing[48,49]. These findings indicate that OPCs deficient in BAF155 exhibit abnormal Ca^{2+} dynamics, which may stem from a weakened synaptic transmission between OPCs and neurons.

To functionally verify the presence and activity of the OPC-neuron synaptic connections, we performed whole-cell patch-clamp recordings on YFP^{+} OPCs from healthy control (*Pdgfrα*^{CreER};*Rosa-YFP)* and *Baf155*-deficient mice (*Pdgfrα*^{CreER};*Baf155*$^{fl/fl}$;*Rosa-YFP*) (Fig. S5E). We measured the currents mediated by two major ionotropic glutamate receptors specifically: α-amino-3-hydroxy-5-methyl-4-isoxazole-propionic acid receptor-evoked EPSCs (AMPAR-eEPSC, recorded at −70 mV) and N-Methyl-D-aspartate receptor-evoked EPSCs (NMDAR-eEPSC, recorded at +40 mV), under a fixed stimulus intensity (Fig. S5F). Subsequently, we calculated the AMPA/NMDA current ratio, which serves as a critical and widely accepted measure for assessing synaptic maturation and strength[50,51]. Our result showed a potential reduction in this ratio in *Baf155*-deficient OPCs, suggesting that again, deletion of *Baf155* in OPCs disrupts the synaptic communication between OPCs and neurons (Fig. S5G).

Together, these findings demonstrate that BAF155 plays a critical role in the development of oligodendroglia by facilitating synaptic communication between OPCs and neurons.

BAF155 modulates heterogeneous responses of OPCs to neuronal inputs in distinct brain regions

To further investigate why loss of BAF155 in vivo induces local hypomyelination, we assessed the chromatin regulatory role of BAF155 to its specific synaptic gene targets in the mPFC and hippocampus using ATAC-qPCR (the assay for transposase-accessible chromatin) and ChIP-qPCR. Our results showed significantly higher chromatin accessibility levels of *Gabrg3*, *Adnp* and *Nfia* in hippocampal OPCs than in cortical OPCs (Fig. 6A); meanwhile, the binding of BAF155 to these target genes in hippocampus were greater than those observed in the mPFC, implying that BAF155 exerts a stronger regulation on these target genes in hippocampal OPCs (Fig. 6B). We also conducted qPCR analysis, which confirmed that the expression levels of BAF155-targeted synaptic genes were elevated in the hippocampus compared to the mPFC (Fig. 6C). Furthermore, we assessed the differentially expressed genes in acutely isolated OPCs from mPFC and hippocampus of *Baf155* knockout mice and their non-Cre littermates by RNA-seq (Fig. 6D). Differential gene expression analysis in each brain region revealed unique gene expression changes and enriched molecular functions specific to the mPFC and hippocampus (Fig. 6E). GO enrichment analysis showed that *Baf155*-deletion upregulated extracellular matrix organization and downregulated steroid metabolic processes specifically in the mPFC; while upregulated cell morphogenesis and downregulated cell activation regulation specifically in hippocampus (Fig. S6A, S6B). The upregulated differentially expressed genes (DEGs) in *Baf155* knockout mice were significantly enriched in multiple biological processes, including regulation of nervous system development and regulation of neuronal synaptic plasticity. The downregulated DEGs were associated with dopaminergic

https://doi.org/10.1038/s41467-025-67930-y

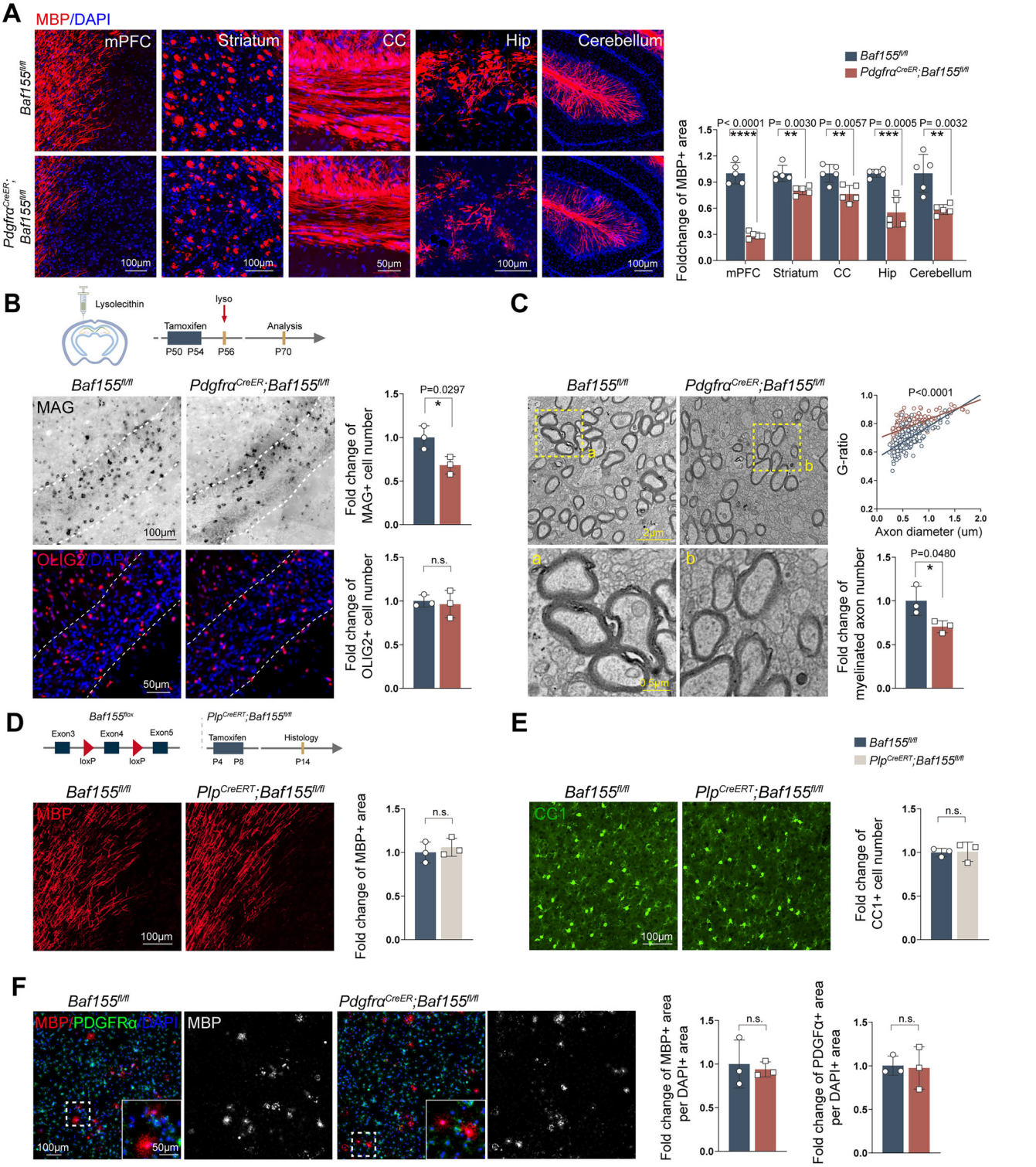

Fig. 3 | Loss of BAF155 impairs OPC differentiation in vivo but not in vitro. **A** Representative images and quantification of MBP staining in the mPFC, striatum, corpus callosum, hippocampus, and cerebellum of *Pdgfra*^{CreER};*Baf155*$^{fl/fl}$ and control mice at P14. Scale bar = 100 μm. $n = 5$ mice. **B** Establishment of a mouse model of lysolecithin-induced demyelinating and the experimental diagram. Representative images of MAG and OLIG2 staining in the corpus callosum and the number of MAG+ and OLIG2+ cells in this region. Scale bar = 100 and 50 μm, respectively; $n = 3$ mice. **C** Electron microscopy image of the corpus callosum, the number of myelinated axons and *G*-ratio in the lysolecithin-induced demyelinating mouse model. Scale bar = 2 μm, $n = 3$ mice. **D** Establishment of *Plp*^{CreERT};*Baf155*$^{fl/fl}$ mouse strain and the experimental diagram. Representative images of MBP staining in the mPFC section and MBP+ area at P14. Scale bar = 100 μm, $n = 3$ mice. **E** Representative images of CC1 staining in the mPFC at P14 and the number of CC1+ cells in this region. Scale bar = 100 μm, $n = 3$ mice. **F** Representative images of MBP/PDGFRα staining in the OPC cultures. The fluorescence intensities were normalized for the total DAPI nuclear area value. Scale bar = 100 μm, $n = 3$ independent experiments. The significance between the two experimental groups was ascertained using the unpaired *t*-test. All statistical tests were two-tailed. Data presented as mean ± SEM; n.s. not significant, $^{*}p < 0.05$, $^{**}p < 0.01$, $^{***}p < 0.001$, $^{****}p < 0.0001$.

https://doi.org/10.1038/s41467-025-67930-y

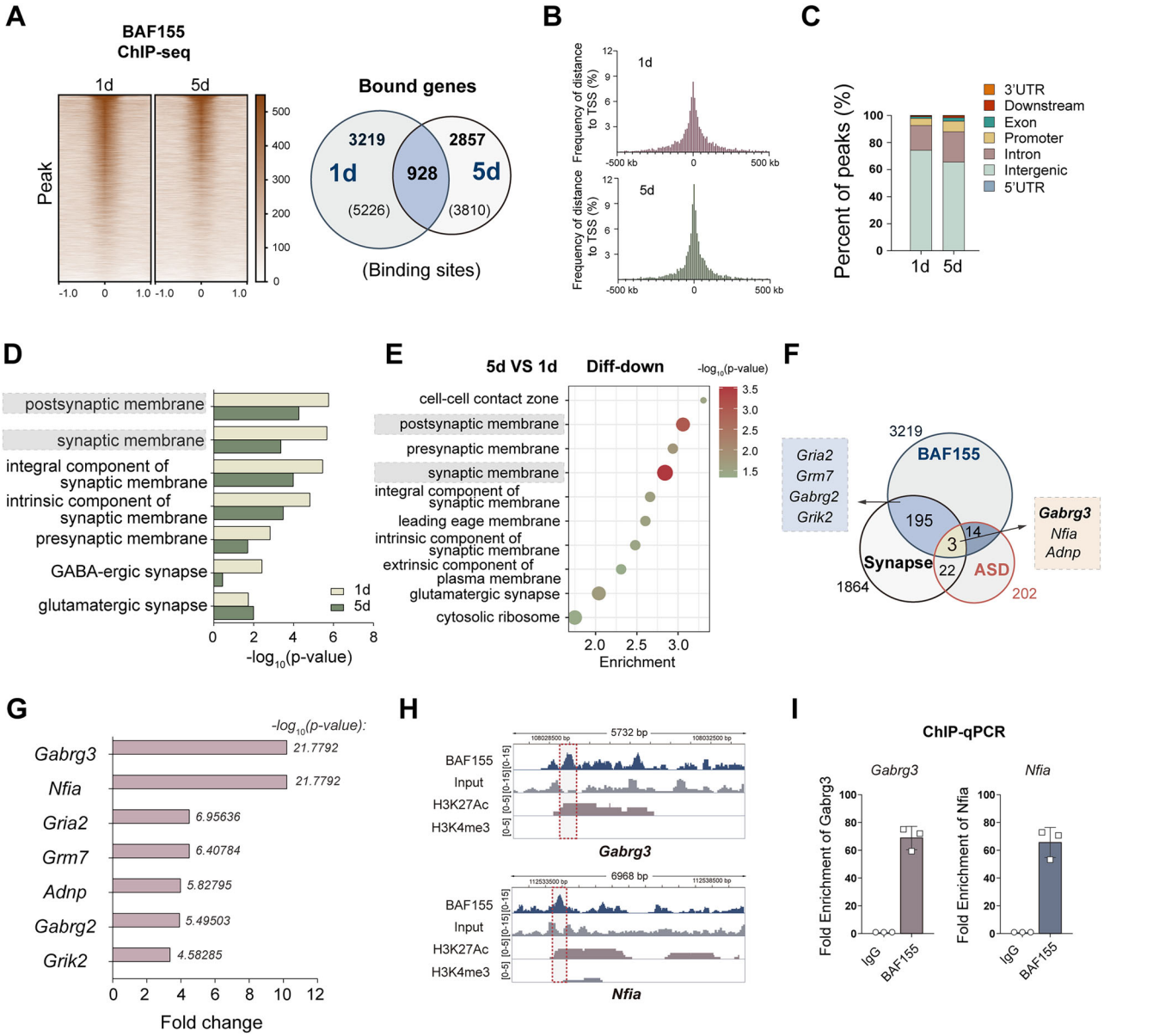

Fig. 4 | BAF155 targets synaptic and ASD-related genes in committed OPCs. **A** Heatmap of BAF155 binding signals in 1 day (the committed OPCs) and 5 days (the OLs) cells. Each line on the *Y*-axis represents a genomic region ±1.0 kb flanking BAF155 summits. Venn diagram of BAF155-binding sites in 1 and 5 days cells. **B** The distribution pattern of BAF155-binding regions according to the distance from their closest transcription start site (TSS) in 1 and 5 days cells. **C** Histogram of the distribution of BAF155 binding peaks in 1 and 5 days cells. **D** Barplot of the GO analysis of the BAF155-bound genes in 1 and 5 days cells. **E** GO analysis of the downregulated genes in the 5 days versus 1 day cells. **F** Venn diagram of the cross-analysis with previously reported ASD susceptibility genes and synaptic genes. **G** Fold enrichment of BAF155 on synaptic genes. **H** Representative ChIP-seq tracks for BAF155 together with active epigenetic marks (H3K27Ac and H3K4me3) of *Gabrg3* and *Nfia* genes in 1 day committed OPCs. **I** Quantification of the ChIP-qPCR of BAF155 on *Gabrg3* and *Nfia* genes in isolated committed OPCs, $n = 3$ biological replicates. The significance between the two experimental groups was ascertained using the unpaired *t*-test. All statistical tests were two-tailed. Data presented as mean ± SEM; n.s. not significant, $^{*}p < 0.05$, $^{**}p < 0.01$.

neurogenesis, axon guidance and synapse pruning (Fig. 6F). Among all identified DEGs, 173 out of 1315 DEGs were affected in both mPFC and hippocampus of *Baf155* knockout mice, 592 out of 1315 were uniquely affected in the mPFC and 377 out of 1315 in the hippocampus (Fig. 6F). As shown in the chord plot (Fig. 6G), *Egr1* (Early growth response 1), *Esr1* (Estrogen Receptor 1 Gene) and *Drd1* (Dopamine D1 receptor), all highly associated with ASD[52–54], were significantly upregulated in both mPFC and hippocampus. However, *Slc17a7* (Solute carrier family 17 member a7), which codes for VGLUT1, a protein responsible for glutamate accumulation into synaptic vesicles[55], and *Neurod1* (Neuronal differentiation 1), which is highly associated with neurogenesis[56], were significantly downregulated in the OPCs from the mPFC region but not in those from the hippocampal region. In contrast, *Lgals3* (Galectin 3), which is essential for OPC differentiation and myelin integrity[57], was specifically downregulated in the hippocampal region.

In line with that, we analyzed the variability of OPC responses to neurotransmitters in various brain regions. The RNA sequencing analysis showed that OPCs from mPFC and hippocampus did not respond in the same manner to the same neurotransmitter GABA (Figs. 6H, S6C, and S6D). When exposed to GABA, *Slc7a11* (Solute carrier family 7 member 11) and *Odc1* (Ornithine decarboxylase 1), which are highly associated with neurodevelopmental disorders and ASD[58,59], were significantly upregulated in the OPCs from the mPFC region but not those from the hippocampus. Furthermore, *Lss* (Lanosterol synthase) and

https://doi.org/10.1038/s41467-025-67930-y

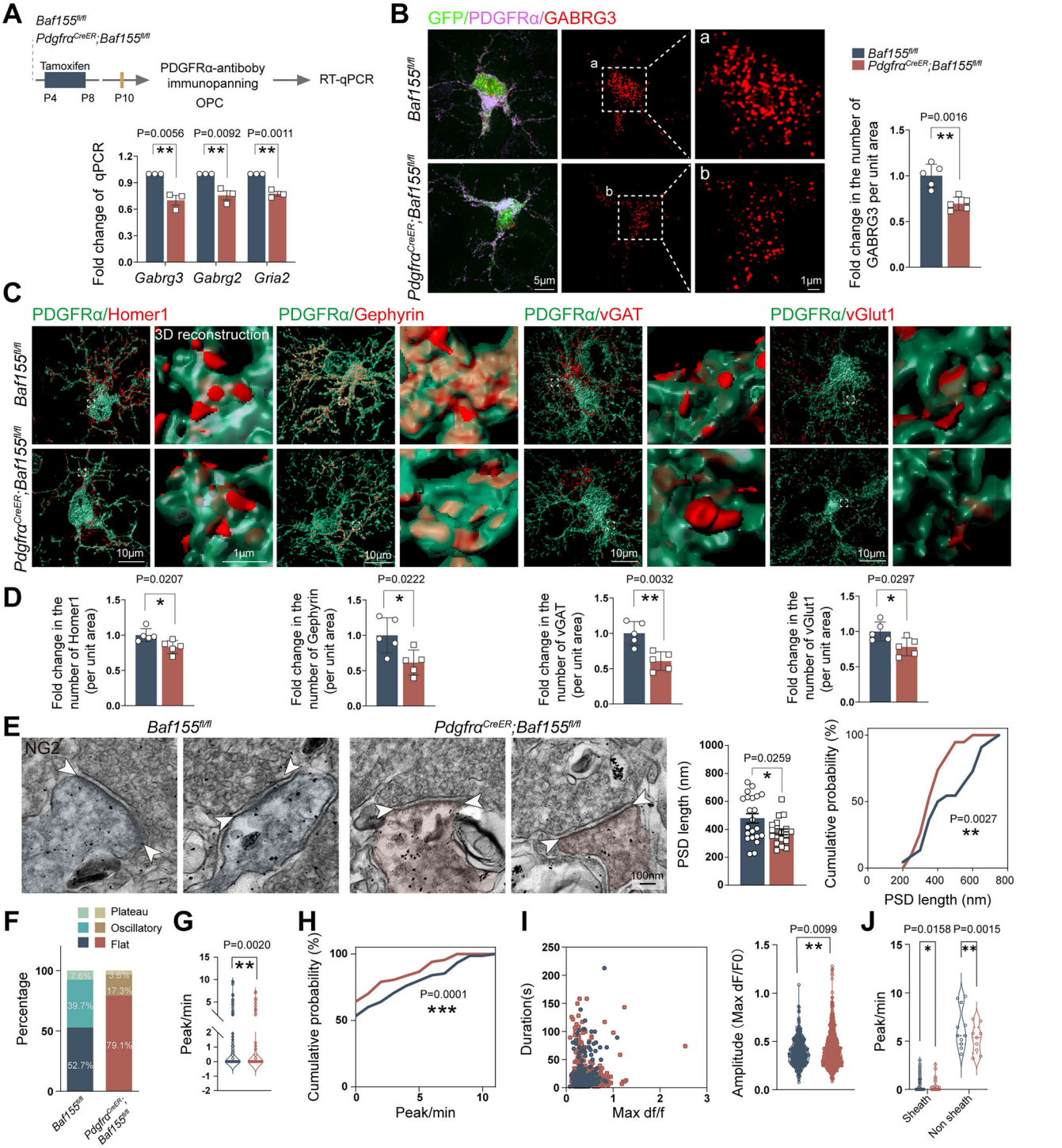

Fig. 5 | BAF155 regulates OPC–neuron synaptic connections. A Quantification of mRNA level of *Gabrg3, Gabrg2,* and *Gria2* in isolated OPCs from *Pdgfra*^{CreER}*;Baf155*$^{fl/fl}$ and control mice, $n = 3$ biological replicates. **B** Representative images in the mPFC of *Pdgfra*^{CreER}*; Rosa-YFP; Baf155*$^{fl/fl}$ and control mice at P14. The number of GABRG3 per unit of PDGFRα+ area. Scale bar = 5 μm, $n = 5$ mice. **C** Surface rendering images in the mPFC at P14. Scale bar = 10 μm. **D** The number of Homer1, Gephyrin, vGAT, and vGLUT1 per unit of PDGFRα+ area. $n = 5$ mice. **E** Representative image of immunoelectron microscopy. The blue or red areas label the NG2+ postsynaptic elements. The arrowheads highlight the postsynaptic density. The length of post-synaptic density (PSD) of the NG2+ postsynaptic elements was graphed as bar plots and a cumulative frequency distribution. $n = 22$ and 19 postsynaptic elements. **F** The quantification of OPC calcium images in *Pdgfra*^{CreER}*;Baf155*$^{fl/fl}$ and control mice. "Oscillatory": 39.67 ± 5.71% (non-Cre wild-type) vs. 17.30 ± 6.65% (*Baf155*-deleted); "plateau": 7.64 ± 4.51% vs. 3.57 ± 2.99%; "flat": 52.96 ± 9.99% vs. 79.12 ± 8.75%. **G** Quantification of calcium wave peak frequency of OPCs. $n = 76$ cells from 3 mice (non-Cre wildtype) and 129 cells from 3 mice (*Baf155*-deleted). **H** Cumulative distribution of calcium wave peak frequency. **I** The maximum duration of the calcium wave of OPCs was plotted against the maximum peak amplitude. Right: the violin plot of maximum peak amplitude. $n = 76$ cells from 3 mice for non-Cre wildtype and 129 cells from 3 mice for *Pdgfra*^{CreER}*;Baf155*$^{fl/fl}$. **J** Quantification of calcium wave peak frequency of sheath-forming and non-sheath cells. $n = 65$ cells for sheath-forming and 11 cells for non-sheath from 3 mice (non-Cre wild-type); $n = 120$ cells for sheath-forming and 9 cells for non-sheath from 3 mice (*Baf155*-deleted). The significance between the two experimental groups was ascertained using the unpaired *t*-test or two-way ANOVA. All statistical tests were two-tailed. Data presented as mean ± SEM; n.s. not significant, $^{*}p < 0.05$, $^{**}p < 0.01$.

https://doi.org/10.1038/s41467-025-67930-y

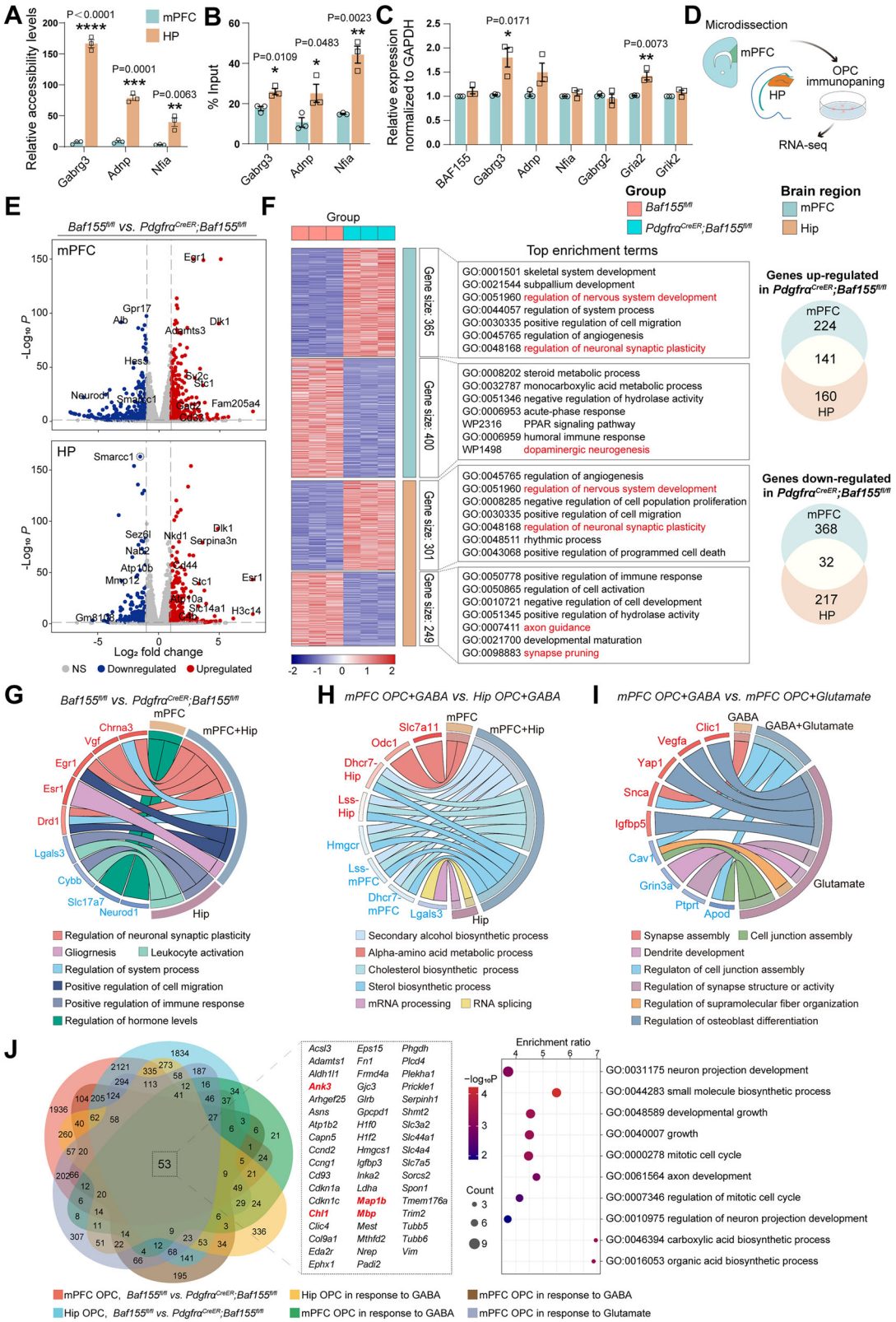

Dhcr7 (7-Dehydrocholesterol reductase), both highly implicated in ASD, mental disorders, and myelination[60,61], were selectively upregulated in the OPCs from the hippocampus but downregulated in the OPCs from mPFC. We also compared the DEGs in OPCs exposed to either GABA or glutamate. As shown by the GO-enrichment analysis, genes related to axonogenesis, dendrite development, synapse development, and cell junction assembly (downregulated) were also significantly different in OPCs between the two groups (Fig. S6E, S6F). As highlighted in the chord plot (Fig. 6I), *Snca* (Alpha-synuclein), highly associated with oligodendrocyte development, myelin formation and mental disorder[62], was upregulated in response to GABA, but not the glutamate; whereas *Igfbp5* (Insulin Like Growth Factor Binding Protein 5), *Vegfa* (Vascular endothelial growth factor A), *Yap1* (Yes-associated protein-1), *Clic1* (Chloride intracellular channel 1), genes also

Fig. 6 | BAF155 regulates heterogeneous responses of OPCs to neuronal inputs in different brain regions. A ATAC assay was performed on the OPCs acutely isolated from the mPFC and hippocampus to elucidate the role of BAF155 in the transcription of *Gabrg3*, *Adnp*, and *Nfia* through regulating chromatin accessibility, $n = 3$ biological replicates. **B** ChIP-qPCR analysis of the comparative enrichment of BAF155 on target genes between OPCs isolated from the mPFC and hippocampus of wild-type mice, $n = 3$ biological replicates. **C** RT-qPCR quantification of mRNA level of *Baf155* and its genomic binding target genes in isolated OPCs from mPFC and hippocampus of wild type mice, $n = 3$ biological replicates. **D** Schematic diagram of the OPC immunopanning workflow from different mouse brain regions. **E** Volcano plot showing differentially expressed genes in OPCs of the mPFC (top) and hippocampus (bottom) region between control and $Pdgfr\alpha^{CreER}$;$Baf155^{fl/fl}$ mice. **F** Heatmap of OPC gene expression profiles in mPFC and Hip, comparing control and $Pdgfr\alpha^{CreER}$;$Baf155^{fl/fl}$ mice. The accompanying bar charts illustrate the numbers of genes upregulated and downregulated in *Baf155*-deletion mice in the mPFC and Hip, respectively. The top enrichment terms for these differentially expressed genes are listed. **G**–**I** Chord plot displaying key genes and the regulation of biological processes in mPFC and Hip of $Pdgfr\alpha^{CreER}$;$Baf155^{fl/fl}$ mice (**G**), isolated OPCs from the mPFC and Hip in response to GABA (**H**), and isolated OPCs from the mPFC in response to excitatory neurotransmitter glutamate and inhibitory neurotransmitter GABA (**I**). **J** Venn diagram of DEGs among OPCs from different conditions and the top enrichment terms of overlap genes. The significance between the two experimental groups was ascertained using the unpaired *t*-test. All statistical tests were two-tailed. Data presented as mean ± SEM; n.s. not significant, $^{*}p < 0.05$, $^{**}p < 0.01$, $^{***}p < 0.001$, $^{****}p < 0.0001$.

associated with oligodendrocyte development and myelin formation[63–65], were upregulated in response to glutamate, but not the GABA. We also compared heterogeneous responses of OPCs derived from various regions to different neurotransmitters, and indicated that the majority of genes exhibited variability under distinct conditions (Fig. 6J).

Collectively, our findings suggest that BAF155 exhibits heterogeneity in OPCs across various brain regions, influencing their responsiveness to neuronal activity and triggering specific gene set expressions in OPCs.

Discussion

In the present study, we reveal that as a chromatin remodeling factor, BAF155 regulates the expression of various synaptic genes in committed OPCs and is essential for establishing synaptic connections and communications between OPCs and neurons. As a master regulator gene, BAF155 coordinates the synaptic and ASD susceptibility genes across different brain regions, affecting local deficits in myelination, which contribute to the onset of ASD-like pathology.

Recent studies extended the pathological relevance of OPCs beyond differentiation to OLs and (re)myelination[13]. In particular, OPCs are found to be synaptically connected with neurons[14,15]. As a chromatin remodeling factor, BAF155 regulates the expression of various synaptic genes in committed OPCs and is essential for establishing synaptic connections and communications between OPCs and neurons. Deletion of *Baf155* from OPCs led to a pronounced decrease in synaptic connections between OPCs and neurons. As shown by super-resolution fluorescence microscopy and immunogold electron microscopy, the pre- and postsynaptic elements decreased in mice lacking BAF155 in OPCs. Therefore, our findings establish a connection between chromatin remodeling and synaptic formation. Considering that neuronal activity enhances myelination[66] and myelin, in turn, facilitates synaptogenesis[67], supports projected neuronal axons and shapes neuronal circuits[16,47,68,69], our results suggest that abnormal OPC-neuron synaptic connections and subsequent myelination could be an early instigator of behavioral defects. In this study, we also found that OPCs from different brain regions exhibit distinct responses to neuronal inputs. This finding deepens our understanding of the heterogeneity of OPCs[70–74]. As a result, it is reasonable to propose that OPC–neuron synaptic connections may give rise to distinct myelin abnormalities (hyper- or hypo-myelination) depending on various CNS regions, ages, and genders in different physiological and pathological states[6,75–78].

As a neurodevelopmental disorder with complex genetic mechanisms, ASD pathogenesis is linked to hundreds of susceptibility genes[79]. Some chromatin remodeling factors, such as CHD8, BRG1, were suggested to contribute to the pathogenesis of ASD[80–82]. However, most of these susceptible genes, when examined individually, fail to recapitulate ASD-like phenotypes in animal models, and many of their underlying mechanisms remain unknown[83–85]. Recently, a growing body of evidence from postmortem and animal studies indicates that white matter, particularly myelin, undergoes alteration at different stages of development in individuals with autism[6,75–77]. Given the well-established roles of myelin in facilitating nerve impulse conduction, promoting synaptogenesis[67], and fine-tuning intracortical network[47], it emerges as a potential key player in ASD pathology[77]. However, the specific contribution of altered myelin to the symptomology seen in ASD also remained unclear. In this study, we successfully induced ASD-like pathology in an OPC-specific knockout mouse model by targeting a newly found ASD susceptibility gene *Baf155*, which encodes a chromatin remodeling factor in the SWI/SNF ATP-dependent BAF complex[23]. Furthermore, we revealed that BAF155 potentially regulates nearly two hundred synaptic genes, which is consistent with the notion that OPC–neuron synaptic contacts contribute to psychiatric disorders[86,87]. Among these synaptic genes, *Gabrg3*, *Nfia*, and *Adnp* are related to ASD[40]. *Gabrg3*, the top-listed synaptic gene enriched in OPCs, was identified as a susceptible gene for autism in the Chinese Han population[42], and is located on the human chromosome locus 15q^{11}-q^{13}, which is a strong candidate region of ASD[88]. Its polymorphism is associated with altered myelination[89,90], and abnormal chromosomal copy number in ASD, accounting for ~10–20% ASD cases[91]. This may further suggest a complex relationship between all three classical pathways of ASD pathogenesis: chromatin remodeling, synaptic formation, and neural projection[79,85]. In this context, the primary chromatin remodeling mechanism for regulating OPC-neuron synaptic connections significantly impacts myelin-supported neural functions, thereby triggering the onset of autistic symptoms[77].

In the present study, we also aimed to explore why BAF155 modulates heterogeneous responses of OPCs to neuronal inputs across different brain regions. In our analysis of DEGs, OPCs exhibit a regional heterogeneity in BAF155 chromatin regulation, along with a unique ability to regulate synaptic gene expression. In line with that, OPC may respond to neurotransmitters in different brain regions. Glutamatergic (AMPA/NMDA) and GABAergic ($GABA_A$/$GABA_B$) receptors are expressed by OPCs[28,92], allowing them to sense activity-dependent release of the two principal CNS neurotransmitters. Glutamate promotes OPC migration, and in later stages, drives differentiation and myelination[93,94]. GABA-induced $GABA_A$ activation inhibits OPC proliferation and reduces myelin thickness, while $GABA_B$ activation stimulates OPC proliferation and migration[95,96]. Additionally, our cross-analysis of DEGs in relation to various regions and neurotransmitters further indicated that although the majority of genes exhibited variability under distinct conditions, 53 overlapping genes were consistently dysregulated, such as *Ank3* (Ankyrin-3[97]), *Chl1* (Close Homolog of L1[98]), *Map1b* (microtubule-associated protein 1b[99]), and *Mbp*[100]. All of these genes are linked to the development of oligodendroglial and neuronal cells, as well as to the pathogenesis of psychiatric disorders. Overall, we suggest that there is a network effect of neuronal activity on OPCs. Neuronal activity, mediated by the release of GABA and glutamate, provides an instructional signaling "code" to OPCs; various patterns of "code" regulate OPCs to differentiate and

myelinate in ways that are specifically aligned with the needs of the local circuit. The chromatin remodeling factor BAF155, the essential regulator, enables OPCs to accurately interpret these neuronal "codes". When BAF155 is deleted, OPC–neuron synaptic connection is disrupted; as a result, this impaired connection prevents OPCs from sensing the neuronal "code" properly, which in turn affects their ability to execute appropriate transcriptional responses and myelinating programs.

We acknowledge the limitations of the present study. The heterozygous BAF155 knockout produces a modest but statistically significant effect, and the mechanisms underlying the overall reduction of oligodendrocyte lineage cells remain unclear. Although using homozygous mutants is a strategy consistent with previous studies on risk genes, it may limit the direct translatability of our findings to human patients. Because of the technical challenges of the OPC patch-clamp, we were able to record three OPCs in each group under identical stimulus conditions. The genes identified on the OPC side are associated with oligodendroglial and neuronal development, as well as the pathogenesis of ASD; however, establishing them as essential mediators linking BAF155, neuronal activity, and disease is far more intricate. Nevertheless, we believe it would be beneficial for future studies to manipulate one of these neurotransmitter receptors on OPCs, correlate genotype–phenotype data with patient cohorts, and integrate multi-omics analyses to further bridge the gap between mouse models and humans.

In summary, our findings deepen our understanding of the cooperation between OPCs and neurons, implying that abnormal synaptogenesis between these two cell types could be an early instigator of the pathogenesis of ASD.

Methods

All animal studies were performed under the guidelines of the laboratory animal welfare and ethics committee of the Third Military Medical University (AMUWEC20223048). All mice were housed in a temperature- and humidity-controlled environment with free access to standard chow and water and on a 12 h/12 h light/dark cycle.

Mice

Our study examined male and female animals, and similar findings are reported for both sexes.

Pdgfrα^{CreER} and Plp^{CreERT}. *Pdgfrα^{CreER}* mice were acquired from Dr. Stephen Fancy at the University of California, San Francisco[101]. *Plp^{CreERT}* mice (JAX lab, Catalog #005975) were purchased from The Jackson Laboratory (USA).

Baf155$^{fl/fl}$. *Baf155*-flox mice were generated by inserting a loxP site on both sides of exon 4 of the Baf155 gene using CRISPR-Cas9 technology by Biocytogen Pharmaceuticals (Beijing) Co., Ltd (China). The mice were then crossed with *Nestin^{CreERT2}* (JAX lab, Catalog #016261), *Pdgfrα^{CreER}*, and *Plp^{CreERT}* mice to generate *Pdgfrα^{CreER};Baf155$^{fl/fl}$* and *Plp^{CreERT}; Baf155$^{fl/fl}$* conditional knockout mice.

Pdgfrα^{CreER}; Rosa-YFP. Rosa-YFP reporter mice (JAX lab, Catalog #006148) were acquired from Dr. Stephen Fancy at the University of California, San Francisco[102]. These mice were crossed with the *Pdgfrα^{CreER}* and *Baf155*-flox mice to specifically label the recombined OPCs.

Nestin^{CreERT2}. *Nestin^{CreERT2}* mice (Catalog #016261) were crossed with *Baf155$^{fl/fl}$* mice to generate *Nestin^{CreERT2}:Baf155$^{fl/+}$* mice.

Mice were administered tamoxifen (10 mg/kg/day, gavage) for 5 consecutive days from postnatal (P)4 to P8 to induce cre-mediated reorganization. To ensure comparability between experimental and control mice, all genotypes of mice were given tamoxifen.

Primary OPC cultures

Rat OPC culture. Primary rat OPCs were cultured using our previous publication[103]. Briefly, cells from P0-3 rat brains were seeded in Dulbecco's modified Eagle Medium (DMEM, Gibco) supplemented with 10% fetal bovine serum (FBS) until confluent. OPCs were detached by the addition of 0.04% EDTA in PBS and repetitive rocking. Then, OPC proliferation medium was used for 2 days to culture the OPCs on a PDL-coated surface. PDGF-AA (10 ng/ml, Peprotech, 100-13A) was removed from the culture medium when OPC differentiation was induced.

Mouse OPC culture. Mouse OPCs were isolated from P10 mice using a modified immunopanning technique based on a previously published method[104]. Briefly, either specific regions or the entire mouse brain were homogenized and digested with 1 mg/mL papain and DNase I at 37 °C for 1 h, with the digestion terminated by adding ovomucoid to inhibit the enzymatic activity. After trituration, the resulting cell suspension was incubated with primary PDGFRα antibody (Abcam, Cat# ab96569), diluted in the panning buffer, for 30 min at room temperature to bind OPCs specifically. The cell suspension was then transferred into a pre-coated secondary antibody dish, and incubated for another 30 min to allow the OPCs to adhere selectively. Then, the panning buffer was used to wash away the non-adherent cells, and the adherent OPCs were released from the panning dish using 0.05% trypsin and cultured in poly-D-lysine-coated 10-cm dishes or 24-well plates with coverslips for further applications.

Behavior tests

Behavioral tests were performed on 6–8-week-old male mice. All mice were acclimatized to the behavioral test apparatus with free access to food and water, and housed on a 12 h/1 h light/dark cycle. Mice were handled daily for 5 days before the test. The apparatus was wiped with 80% alcohol between each trial. All tests were conducted between 9 a.m. and 6 p.m. The experimenters were blinded to the grouping. VisuTrack Animal Behavior Analysis Software (Shanghai XinRuan) was used for data collection and analysis.

The three-chamber test. The three-chamber test was used to assess the sociability and social novelty preference. The apparatus consisted of three chambers: the center, the left, and the right chambers. The test mice were first placed in the center chamber and allowed to explore the three chambers freely for 10 min to familiarize themselves with the environment. In the first phase (sociability test, indicated as Stranger1-Object, S1-O, in figures), an unfamiliar mouse of the same age and sex was randomly placed in the cage located in either the left or right chamber, and the baffles of the two chambers were opened to allow the test mouse to explore freely. The sociability was assessed by recording the sniffing time of the test mouse at the caged mouse (Stranger1) and the empty cage (Object). In the second phase (social novelty preference test, indicated as Stranger1–Stranger2, S1–S2 in figures), a new unfamiliar mouse was placed in the vacant cage on the other side, and the sniffing time on the stranger2 versus the stranger1 was recorded.

The self-grooming test. The self-grooming test was used to assay repetitive behaviors in mice. Test mice were placed in a transparent chamber and allowed to freely explore and familiarize themselves with the environment for 10 min before being recorded for another 10 min. The cumulative time of self-grooming of the mice was calculated.

Novel object recognition test. A novel object recognition test was used to assess short-term memory function. Two days before the experiment, mice were placed in the chamber (25 × 25 × 40 cm) for 10 min each day to acclimatize to the test environment. During the trial, two identical objects were placed in the chamber for the mouse to explore for 5 min. After two hours, one of the objects was replaced with

a new one with a different shape and color for the mouse to explore for 5 min. The times spent on the new versus the old object were recorded.

Open field test. The open-field test was used to assess the motor ability, as well as anxiety-like behavior, of mice. Test mice were placed in the center of the arena (50 × 50 cm) and allowed to explore freely for 15 min. The total distance traveled by the mice, and the time and distance traveled in the central area, were recorded. The time or distance traveled in the center area reflects anxiety-like behavior. Data collection and analysis were performed with the VisuTrack Animal Behavior Analysis Software.

Elevated plus maze. The elevated plus maze test was used to assess anxiety-like behavior in mice. The mouse was placed in the center of the crossing and faced the open arms. Mice were allowed to explore for 10 min. Anxiety-like behavior was assessed by comparing the time or distance traveled in the closed arms.

Tail suspension test. The tail suspension test was used to measure depression-associated behavior. The mouse tail was secured to the top of the test chamber (55 × 15 × 11.5 cm) with adhesive tape to keep the head approximately 25 cm from the bottom of the chamber for 10 min. The time of immobility was quantified.

Forced swimming test. The forced swimming test was used to assess depression-associated behavior in mice. The water depth in the arena (10 × 25 cm) was 15 cm, and the water temperature was 25 °C. The mouse was placed in the arena for 6 min and the time of fatigue was recorded.

Lysolecithin-induced demyelinating mouse model

A mouse model of lysolecithin-induced demyelinating has been described in our previous papers[105,106]. Briefly, for the demyelination mouse model, tamoxifen was administered continuously from P50 to P54. At P56, mice were anesthetized by isoflurane (2–3%); after exposing the skull, 1.5 µl 1% lysolecithin (Sigma-Aldrich, L0906) was injected into the corpus callosum (1.04 mm lateral and 1.0 mm posterior to the bregma, depth: −1.62 mm). Two weeks later, brain tissue was harvested for immunofluorescence staining and in situ hybridization.

Real time-PCR

Total RNA was extracted using the RNeasy Plus Mini Kit (Qiagen, Cat# 74134). The PrimeScript RT Reagent Kit (Takara) was used for reverse transcription. The Accurate 96 Real Time PCR System (DLAB) and FastStart Universal SYBR Green Master Mix (Roche, 04913850001) were used for the qPCR experiment. All primer sequences are presented in Supplementary Data 2.

In situ hybridization

In situ hybridization was performed as previously described[105]. Brains were fixed with 4% PFA and cryoprotected in 30% sucrose with 0.1% diethyl pyrocarbonate before sectioning at 20 µm. The brain sections were incubated with digoxigenin (DIG)-labeled antisense MAG probe at 65 °C overnight, followed by the incubation with anti-DIG-AP Fab fragments antibody (1:1000, Sigma-Aldrich, 11093274910) at 4 °C overnight and NBT/BCIP alkaline phosphatase combination (Sigma-Aldrich, 11681451001) for 4 h at 37 °C or overnight at room temperature. The cells expressing the genes of interest displayed dark purple staining.

Immunohistochemistry

Mice were intracardially perfused with 4% PFA, and brains were removed and fixed in 4% PFA overnight at 4 °C. The brains were cryoprotected with 30% sucrose for 3 days before being cryosectioned at 20 µm. Sections were blocked with 5% bovine serum albumin (BSA) with 0.25% Triton-X 100 for 2 h at room temperature before being incubated with primary antibodies overnight at 4 °C, followed by secondary antibodies for one hour at room temperature. The primary antibodies include: Rat anti-MBP (1:500, Millipore, MAB395); Mouse anti-CC1 (1:500, Calbiochem, OP80); Guinea anti-vGlut1 (1:2000, Synaptic Systems, 135304); Mouse anti-vGAT (1:1000, Synaptic Systems, 131011); Rabbit anti-Homer1 (1:1000, Synaptic Systems, 160003); Mouse anti-Synapsin-1 (1:1000, Cell Signaling Technology, 5297); Goat anti-PDGFRα (1:500, R&D, AF1062); Mouse anti-Olig2 (1:500, Millipore, MABN50); Rabbit anti-Olig2 (1:500, Millipore, AB9610); Rabbit anti-Ki67 (1:1000, Thermo, MA514520); Goat anti-GFP (1:500, Abcam, ab5450). The Olympus VS200 Research Slide Scanner (Olympus) and Ixplore SpinSR confocal microscope (Olympus) were used for imaging. Fluorescent images were analyzed using the CellSens (Olympus) and ImageJ (NIH, USA).

Electrophysiology

The N-methyl-D-glucamine (NMDG) protective recovery method was used to prepare brain slices[107]. NMDG-HEPES aCSF contains (in mM): 92 NMDG, 2.5 KCl, 1.25 NaH_2PO_4, 30 $NaHCO_3$, 20 HEPES, 25 glucose, 2 thiourea, 5 Na-ascorbate,3 Na-pyruvate, 0.5 $CaCl_2{\cdot}2H_2O$, and 10 $MgSO_4{\cdot}7H_2O$. HEPES with aCSF contains (in mM): 92 NaCl, 2.5 KCl, 1.25 NaH_2PO_4, 30 $NaHCO_3$, 20 HEPES, 25 glucose, 2 thiourea, 5 Na-ascorbate, 3Na-pyruvate, 2 $CaCl_2{\cdot}2H_2O$, and 2 $MgSO_4{\cdot}7H_2O$. For spontaneous excitatory postsynaptic currents (sEPSCs) and inhibitory postsynaptic currents (sIPSCs) recording, whole-cell patch-clamp recordings were performed using borosilicate glass pipettes. sEPSCs were recorded at a holding potential of −70 mV, and sIPSCs were recorded at a holding potential of +10 mV in regular ACSF. As described previously[108], for isolating miniature excitatory postsynaptic currents (mEPSCs), we continuously infused sodium channel blocker tetrodotoxin (TTX, 1 µM; MLC, MBZ10175) into the ACSF. For recording miniature inhibitory postsynaptic currents (mIPSCs), we used a special pipette solution containing CsCl and administered the AMPA receptor antagonist NBQX (10 µM; MCE, HY-15068) and NMDA receptor antagonist D-AP5 (50 µM; MCE, HY-100714A) or TTX (1 µM) + NBQX (10 µM) + D-AP5 (50 µM) into the ACSF throughout the recording. We clamped membrane potentials at −60 mV to record both mEPSCs and mIPSCs for at least 15 min. For voltage-clamp recordings on OPCs[15], an individual slice was transferred to the recording chamber with the external ACSF containing (in mM): 125 NaCl, 2.5 KCl, 1.25 NaH_2PO_4, 26 $NaHCO_3$, 10 glucose, 2 $CaCl_2{\cdot}2H_2O$, and 1 $MgSO_4{\cdot}7H_2O$. The patch pipette was injected with internal solution (in mM): 135 Cs methanesulfonate, 8 NaCl, 10 HEPES, 2 Mg_2ATP, 0.3 Na_3GTP, 0.1 Spermine, 7 phosphocreatine, and 0.3 EGTA. AMPAR-mediated EPSCs were recorded at −70 mV, NMDAR-mediated EPSCs were recorded for 100 ms at +40 mV. As a stimulation electrode, the electrode was inserted into the stratum radiatum of the CA1 area. A MultiClamp 700B amplifier and pCLAMP10 software were used for electrophysiology (Axon Instruments). Minianalysis and Clampfit software were used for data analysis. The AMPA/NMDA ratio was calculated as described previously[50,51].

Immunogold labeling

Mice were perfused intracardially with PBS followed by pre-cold 4% PFA, and the brains were processed by Vibratome (submerged in 0.1 M PBS) to obtain 50 µm free-floating sections. Sections were postfixed with 4% PFA with 0.1% glutaraldehyde in 0.1 M PB for 2 h, washed with 0.1 M PB for 10 min thrice. The residual fixatives were then quenched with 50 mM glycine in 0.1 M PB for 30 min. Sections were washed with 0.1 M PB for 10 min, permeabilized in 0.05% Triton-X100:PB for 15 min, washed again with 0.1 M PB for 15 min, and incubated in blocking buffer (0.1 M PBS with 0.1% BSA-CTM) for 1.5 h. Sections were then incubated with primary antibody (Rabbit-anti-NG2 (1:200, Millipore, AB5320)) at 4 °C overnight, washed with blocking buffer 6 × 10 min,

and incubated with 1.4-nm gold-conjugated secondary antibody (Nanoprobes) overnight. Sections were then washed with blocking buffer 6 × 10 min, 0.1 M PB 3 × 10 min, and postfixed in 2.5% glutaraldehyde for 4 h, followed by washing with 0.1 M PB 3 × 10 min, ddH_2O 6 × 5 min, sodium citrate (pH 7.0) 3 × 5 min, before being subjected to silver enhancement with the HQ Silver Kit (Nanoprobes). Immunolabelled sections were rinsed in ddH_2O 6 × 10 min, post-fixed with 1% osmium tetroxide in PB for 1 h, and then incubated in 2% uranyl acetate in ddH_2O for 40 min in the dark. Sections were dehydrated in graded ethanol, then acetone series, and finally flat-embedded in Epon 812. After polymerization, flat-embedded sections were examined under a light microscope. Serial ultrathin (~70–90 nm) sections were cut with an ultramicrotome (Leica EM UC6, Germany) using a diamond knife (Diatome) and mounted on formvar-coated mesh grids (6–8 sections per grid). They were observed under a Tecnai G2 Spirit 120 kV transmission electron microscope at the Center of Cryo-Electron Microscopy, Zhejiang University.

Calcium imaging

As described previously[109], isolated OPCs were incubated with calcium probe Rhod-5 at 37 °C in the dark for 30 min. Confocal images were captured by an Ixplore SpinSR confocal microscope (Olympus) at 200 ms per frame and analyzed by the ImageJ software.

Gene expression analysis from online mouse scRNA-seq platform

The Mouse Whole-Brain Transcriptomic Cell Type Atlas data were accessed via the Allen Institute for Brain Science (https://portal.brain-map.org)[31]. The dataset comprises scRNA-seq data from approximately 4 million cells, covering diverse cell types across the entire mouse brain. To examine the gene expression of the target genes *Baf155*, *Gabrg3*, and Gabr subtypes, we used the portal's search function and interactive features to visualize the transcriptomic data. The platform provides UMAP plots, heatmaps showing the expression of Baf155 and Gabrg3 across different cell types. Ridgeline plots were generated with R "ggridges" package with the data acquired from The Mouse Whole-Brain Transcriptomic Cell Type Atlas.

Assay for transposase-accessible chromatin (ATAC assay)

A chromatin accessibility kit was purchased from Abcam (ab185901), and the assay was performed according to the manufacturer's instructions[110]. Briefly, OPCs were isolated from the mouse hippocampus and mPFC by immunopanning. Then, OPCs were incubated on ice, vortexed, and centrifuged (5000 × *g*, 5 min). After cell lysis, the OPC chromatin was treated with a nuclease mix, and OPC DNA was purified (250 μL binding buffer, two washes with 200 μL wash buffer, elution with 20 μL elution buffer), and subjected to qPCR for region-specific analysis of chromatin accessibility. All primer sequences are presented in Supplementary Data 2.

Chromatin immunoprecipitation-sequencing (ChIP-seq) and qPCR

ChIP-seq technology is used to determine BAF155-binding sites as described previously[111]. In cells, protein–DNA complexes were immobilized using formaldehyde at a final concentration of 1% to preserve the protein–DNA interactions. The crosslinking process was then terminated by adding glycine, typically at a concentration of 0.125 M. Next, cell membranes were disrupted with lysis buffer to release the nuclear material. The chromatin was sheared into small fragments, usually ranging from 200 to 1000 base pairs, through ultrasonic fragmentation. This was followed by enriching the protein–DNA complexes using the BAF155 antibody (Cell Signaling Technology, catalog number 11956). The BAF155 antibody was bound to Protein A + G magnetic beads (Magna ChIP™, catalog number 16-663), and the sonicated samples were incubated overnight with the antibody-bound beads. After incubation, unbound material was removed, and DNA fragments were released from the immunoprecipitation complexes. The purified DNA underwent end repair and splice addition, followed by amplification using PCR to generate a sequencing library. Once the library was tested and validated, it was sequenced using the Illumina HiSeq platform. Following ChIP-seq sequencing, raw reads were obtained and filtered to remove junctions. The data were decontaminated and aligned to the reference genome. Finally, high-quality-mapped reads with a mean Phred quality score (MPAQ) of 30 or greater were used for subsequent analysis. ChIP-qPCR was adopted to quantify the presence and abundance of protein–DNA complexes at specific DNA sequences[112]. Following similar procedures, the protein–DNA complexes were collected, and the DNA was released by reversing the cross-links through heating, typically overnight at 65 °C. Afterward, the DNA samples were purified and analyzed using qPCR. All primer sequences are presented in Supplementary Data 2.

RNA-sequencing and analysis

OPCs were isolated by immunopanning, and RNA was extracted from the isolated cells by Trizol (Thermo, Cat. No. 15596026) according to the manufacturer's protocol. RNA-seq was performed by the Beijing Genomics Institute (BGI). Raw RNA sequencing data in FASTQ format were initially processed using quality control steps. Adapter sequences and low-quality reads were removed using tools such as Trim Galore to ensure the integrity of the downstream analysis. The clean data were then aligned to GRCm38 for genome reference. Normalization of gene expression was performed by transferring the read counts to FPKM values. Gene expression levels were quantified, and differential expression analysis was performed using DESeq2. Genes with adjusted *p*-values below 0.05 were considered statistically significant. Data visualization and downstream analysis were conducted using R, with functional enrichment analysis performed using the ClusterProfiler package.

Statistics

Quantification of cell numbers. The number of immunostaining-positive cells was manually counted and normalized to the area of the region of interest. Only cells with visible cell bodies were included.

Quantification of fluorescence intensity or positive area. Quantification of fluorescence intensity or the fluorescence-positive area was performed using the Fiji software, where a threshold was set to distinguish the positive fluorescence signals, followed by the measurement of fluorescence intensity and the positive area percentage within the region of interest. The same threshold was set for different experiment groups in the same batch. For the analysis of representative images of MBP/PDGFRα staining in OPC cultures, the fluorescence intensities were normalized for the total DAPI nuclear area value.

Quantification of synaptic element immunostaining in OPC. The analysis was performed by Imaris 9.0 according to a previous publication[113]. Briefly, the OPC surface was reconstructed based on the PDGFRα signal, which was then used to mask the synaptic element staining. The surface rendering was performed on the masked synaptic element signal, and the number of objects was quantified.

The GraphPad Prism program 9.0 (GraphPad program, San Diego, CA, USA) was used to establish statistical significance between groups. The data were reported as means ± standard error of the mean (SEM). The significance between the two experimental groups was ascertained using the unpaired *t*-test. All statistical tests were two-tailed. *p*-values were regarded as statistically significant if they were <0.05. Significant statistical results are indicated as: $^{*}p < 0.05$, $^{**}p < 0.01$, $^{***}p < 0.001$, $^{****}p < 0.0001$. Data distribution was assumed to be normal, but this was not formally tested. Although sample sizes were not predetermined using statistical techniques, our numbers are comparable to those reported in previous studies. Each experiment has been conducted at least three times.

Reporting summary

Further information on research design is available in the Nature Portfolio Reporting Summary linked to this article.

Data availability

RNA-seq upon GABA and Glutamate and ChIP-seq data of BAF155 in this manuscript have been deposited in the NCBI GEO database under the accession numbers GSE282099 and GSE282098. Accession numbers are listed in the key resources table. ChIP-seq H3K27Ac and H3K4me3 data were obtained from samples GSE42447, GSE42454, and GSE84011. Any additional information required to reanalyze the data reported in this paper is available from the lead contact upon request. Source data are provided with this paper.

References

1. Baio, J. et al. Prevalence of autism spectrum disorder among children aged 8 years—autism and developmental disabilities monitoring network, 11 sites, United States, 2014. *MMWR Surveill. Summ.* **67**, 1–23 (2018).
2. Fetit, R., Hillary, R. F., Price, D. J. & Lawrie, S. M. The neuropathology of autism: a systematic review of post-mortem studies of autism and related disorders. *Neurosci. Biobehav. Rev.* **129**, 35–62 (2021).
3. Parellada, M. et al. The neurobiology of autism spectrum disorders. *Eur. Psychiatry* **29**, 11–19 (2014).
4. Ma, D. Q. et al. Identification of significant association and gene–gene interaction of GABA receptor subunit genes in autism. *Am. J. Hum. Genet.* **77**, 377–388 (2005).
5. Carlisi, C. O. et al. Comparative multimodal meta-analysis of structural and functional brain abnormalities in autism spectrum disorder and obsessive-compulsive disorder. *Biol. Psychiatry* **82**, 83–102 (2017).
6. Phan, B. N. et al. A myelin-related transcriptomic profile is shared by Pitt–Hopkins syndrome models and human autism spectrum disorder. *Nat. Neurosci.* **23**, 375–385 (2020).
7. Rubenstein, J. L. & Merzenich, M. M. Model of autism: increased ratio of excitation/inhibition in key neural systems. *Genes Brain Behav.* **2**, 255–267 (2003).
8. Courchesne, E. & Pierce, K. Why the frontal cortex in autism might be talking only to itself: local over-connectivity but long-distance disconnection. *Curr. Opin. Neurobiol.* **15**, 225–230 (2005).
9. Hussman, J. P. Suppressed GABAergic inhibition as a common factor in suspected etiologies of autism. *J. Autism Dev. Disord.* **31**, 247–248 (2001).
10. Son, E. Y. & Crabtree, G. R. The role of BAF (mSWI/SNF) complexes in mammalian neural development. *Am. J. Med. Genet. C Semin. Med. Genet.* **166C**, 333–349 (2014).
11. Sacai, H. et al. Autism spectrum disorder-like behavior caused by reduced excitatory synaptic transmission in pyramidal neurons of mouse prefrontal cortex. *Nat. Commun.* **11**, 5140 (2020).
12. Contractor, A., Ethell, I. M. & Portera-Cailliau, C. Cortical interneurons in autism. *Nat. Neurosci.* **24**, 1648–1659 (2021).
13. Yi, C., Verkhratsky, A. & Niu, J. Pathological potential of oligodendrocyte precursor cells: terra incognita. *Trends Neurosci.* **46**, 581–596 (2023).
14. Fang, L. P. et al. Impaired bidirectional communication between interneurons and oligodendrocyte precursor cells affects social cognitive behavior. *Nat. Commun.* **13**, 1394 (2022).
15. Bergles, D. E., Roberts, J. D., Somogyi, P. & Jahr, C. E. Glutamatergic synapses on oligodendrocyte precursor cells in the hippocampus. *Nature* **405**, 187–191 (2000).
16. Lin, S. C. & Bergles, D. E. Synaptic signaling between GABAergic interneurons and oligodendrocyte precursor cells in the hippocampus. *Nat. Neurosci.* **7**, 24–32 (2004).
17. Li, J., Miramontes, T. G., Czopka, T. & Monk, K. R. Synaptic input and Ca(2+) activity in zebrafish oligodendrocyte precursor cells contribute to myelin sheath formation. *Nat. Neurosci.* **27**, 219–231 (2024).
18. Buchanan, J. et al. Oligodendrocyte precursor cells ingest axons in the mouse neocortex. *Proc. Natl. Acad. Sci. USA* **119**, e2202580119 (2022).
19. Mount, C. W., Yalçın, B., Cunliffe-Koehler, K., Sundaresh, S. & Monje, M. Monosynaptic tracing maps brain-wide afferent oligodendrocyte precursor cell connectivity. *Elife* **8**, https://doi.org/10.7554/eLife.49291 (2019).
20. Auguste, Y. S. S. et al. Oligodendrocyte precursor cells engulf synapses during circuit remodeling in mice. *Nat. Neurosci.* **25**, 1273–1278 (2022).
21. Yu, G. et al. Pathological oligodendrocyte precursor cells revealed in human schizophrenic brains and trigger schizophrenia-like behaviors and synaptic defects in genetic animal model. *Mol. Psychiatry* **27**, 5154–5166 (2022).
22. Zhang, X. et al. NG2 glia-derived GABA release tunes inhibitory synapses and contributes to stress-induced anxiety. *Nat. Commun.* **12**, 5740 (2021).
23. Alver, B. H. et al. The SWI/SNF chromatin remodelling complex is required for maintenance of lineage specific enhancers. *Nat. Commun.* **8**, 14648 (2017).
24. Abbas, E. et al. Conditional loss of BAF (mSWI/SNF) scaffolding subunits affects specification and proliferation of oligodendrocyte precursors in developing mouse forebrain. *Front. Cell Dev. Biol.* **9**, 619538 (2021).
25. Narayanan, R. et al. Loss of BAF (mSWI/SNF) complexes causes global transcriptional and chromatin state changes in forebrain development. *Cell Rep.* **13**, 1842–1854 (2015).
26. Nguyen, H. et al. Epigenetic regulation by BAF complexes limits neural stem cell proliferation by suppressing Wnt signaling in late embryonic development. *Stem Cell Rep.* **10**, 1734–1750 (2018).
27. Sokpor, G., Xie, Y., Rosenbusch, J. & Tuoc, T. Chromatin remodeling BAF (SWI/SNF) complexes in neural development and disorders. *Front. Mol. Neurosci.* **10**, 243 (2017).
28. Moura, D. M. S., Brennan, E. J., Brock, R. & Cocas, L. A. Neuron to oligodendrocyte precursor cell synapses: protagonists in oligodendrocyte development and myelination, and targets for therapeutics. *Front. Neurosci.* **15**, 779125 (2021).
29. Wilfert, A. B. et al. Recent ultra-rare inherited variants implicate new autism candidate risk genes. *Nat. Genet.* **53**, 1125–1134 (2021).
30. Wenderski, W. et al. Loss of the neural-specific BAF subunit ACTL6B relieves repression of early response genes and causes recessive autism. *Proc. Natl. Acad. Sci. USA* **117**, 10055–10066 (2020).
31. Yao, Z. et al. A high-resolution transcriptomic and spatial atlas of cell types in the whole mouse brain. *Nature* **624**, 317–332 (2023).
32. Ferreira, S. et al. Amyloidosis is associated with thicker myelin and increased oligodendrogenesis in the adult mouse brain. *J. Neurosci. Res.* **98**, 1905–1932 (2020).
33. Zeisel, A. et al. Brain structure. Cell types in the mouse cortex and hippocampus revealed by single-cell RNA-seq. *Science* **347**, 1138–1142 (2015).
34. Fang, M., Chen, L., Tang, T., Qiu, M. & Xu, X. The committed oligodendrocyte precursor cell, a newly-defined intermediate progenitor cell type in oligodendroglial lineage. *Glia* **71**, 2499–2510 (2023).
35. Vasa, R. A. & Mazurek, M. O. An update on anxiety in youth with autism spectrum disorders. *Curr. Opin. Psychiatry* **28**, 83–90 (2015).
36. Fancy, S. P., Chan, J. R., Baranzini, S. E., Franklin, R. J. & Rowitch, D. H. Myelin regeneration: a recapitulation of development? *Annu. Rev. Neurosci.* **34**, 21–43 (2011).

37. Niu, J. et al. Oligodendroglial ring finger protein Rnf43 is an essential injury-specific regulator of oligodendrocyte maturation. *Neuron* **109**, 3104–3118.e3106 (2021).
38. Arnett, H. A. et al. bHLH transcription factor Olig1 is required to repair demyelinated lesions in the CNS. *Science* **306**, 2111–2115 (2004).
39. Marie, C. et al. Oligodendrocyte precursor survival and differentiation requires chromatin remodeling by Chd7 and Chd8. *Proc. Natl. Acad. Sci. USA* **115**, E8246–E8255 (2018).
40. Adak, P., Sinha, S. & Banerjee, N. An association study of gamma-aminobutyric acid type A receptor variants and susceptibility to autism spectrum disorders. *J. Autism Dev. Disord.* **51**, 4043–4053 (2021).
41. Li, X., Zou, H. & Brown, W. T. Genes associated with autism spectrum disorder. *Brain Res. Bull.* **88**, 543–552 (2012).
42. Wang, L. et al. Association study and mutation sequencing of genes on chromosome 15q11-q13 identified GABRG3 as a susceptibility gene for autism in Chinese Han population. *Transl. Psychiatry* **8**, 152 (2018).
43. Yang, S. et al. GABA(A) receptor subunit gene polymorphisms predict symptom-based and developmental deficits in Chinese Han children and adolescents with autistic spectrum disorders. *Sci. Rep.* **7**, 3290 (2017).
44. Yu, Y. et al. Olig2 targets chromatin remodelers to enhancers to initiate oligodendrocyte differentiation. *Cell* **152**, 248–261 (2013).
45. Chen, F. X., Smith, E. R. & Shilatifard, A. Born to run: control of transcription elongation by RNA polymerase II. *Nat. Rev. Mol. Cell Biol.* **19**, 464–478 (2018).
46. Ou, Z. et al. Olig2-targeted G-protein-coupled receptor Gpr17 regulates oligodendrocyte survival in response to lysolecithin-induced demyelination. *J. Neurosci.* **36**, 10560–10573 (2016).
47. Benamer, N., Vidal, M., Balia, M. & Angulo, M. C. Myelination of parvalbumin interneurons shapes the function of cortical sensory inhibitory circuits. *Nat. Commun.* **11**, 5151 (2020).
48. Krasnow, A. M., Ford, M. C., Valdivia, L. E., Wilson, S. W. & Attwell, D. Regulation of developing myelin sheath elongation by oligodendrocyte calcium transients in vivo. *Nat. Neurosci.* **21**, 24–28 (2018).
49. Baraban, M., Koudelka, S. & Lyons, D. A. Ca (2+) activity signatures of myelin sheath formation and growth in vivo. *Nat. Neurosci.* **21**, 19–23 (2018).
50. Thomas, M. J., Beurrier, C., Bonci, A. & Malenka, R. C. Long-term depression in the nucleus accumbens: a neural correlate of behavioral sensitization to cocaine. *Nat. Neurosci.* **4**, 1217–1223 (2001).
51. Basilico, B. et al. Microglia shape presynaptic properties at developing glutamatergic synapses. *Glia* **67**, 53–67 (2019).
52. Rapanelli, M. et al. Targeting histone demethylase LSD1 for treatment of deficits in autism mouse models. *Mol. Psychiatry* **27**, 3355–3366 (2022).
53. Sathyanarayana, S. et al. A pilot study of the association between genetic polymorphisms involved in estrogen signaling and infant male genital phenotypes. *Asian J. Androl.* **14**, 766–772 (2012).
54. Mariggio, M. A. et al. DRD1 and DRD2 receptor polymorphisms: genetic neuromodulation of the dopaminergic system as a risk factor for ASD, ADHD and ASD/ADHD overlap. *Front. Neurosci.* **15**, 705890 (2021).
55. Bellocchio, E. E., Reimer, R. J., Fremeau, R. T. Jr. & Edwards, R. H. Uptake of glutamate into synaptic vesicles by an inorganic phosphate transporter. *Science* **289**, 957–960 (2000).
56. Hsieh, J., Nakashima, K., Kuwabara, T., Mejia, E. & Gage, F. H. Histone deacetylase inhibition-mediated neuronal differentiation of multipotent adult neural progenitor cells. *Proc. Natl. Acad. Sci. USA* **101**, 16659–16664 (2004).
57. Pasquini, L. A. et al. Galectin-3 drives oligodendrocyte differentiation to control myelin integrity and function. *Cell Death Differ.* **18**, 1746–1756 (2011).
58. Jiang, P. et al. Puerarin attenuates valproate-induced features of ASD in male mice via regulating Slc7a11-dependent ferroptosis. *Neuropsychopharmacology* **49**, 497–507 (2024).
59. Prokop, J. W. et al. Emerging role of ODC1 in neurodevelopmental disorders and brain development. *Genes (Basel)* **12**, https://doi.org/10.3390/genes12040470 (2021).
60. Hubler, Z. et al. Modulation of lanosterol synthase drives 24,25-epoxysterol synthesis and oligodendrocyte formation. *Cell Chem. Biol.* **28**, 866–875 e865 (2021).
61. Miyazaki, S. et al. DHCR7 links cholesterol synthesis with neuronal development and axonal integrity. *Biochem. Biophys. Res. Commun.* **712-713**, 149932 (2024).
62. Hentrich, T. et al. Increased expression of myelin-associated genes in frontal cortex of SNCA overexpressing rats and Parkinson's disease patients. *Aging (Albany, NY)* **12**, 18889–18906 (2020).
63. Cheng, H. L. & Feldman, E. L. Insulin-like growth factor-I (IGF-I) and IGF binding protein-5 in Schwann cell differentiation. *J. Cell Physiol.* **171**, 161–167 (1997).
64. Hayakawa, K. et al. Vascular endothelial growth factor regulates the migration of oligodendrocyte precursor cells. *J. Neurosci.* **31**, 10666–10670 (2011).
65. Shimizu, T. et al. YAP functions as a mechanotransducer in oligodendrocyte morphogenesis and maturation. *Glia* **65**, 360–374 (2017).
66. de Faria, O. Jr, Gonsalvez, D. G., Nicholson, M. & Xiao, J. Activity-dependent central nervous system myelination throughout life. *J. Neurochem.* **148**, 447–461 (2019).
67. Wang, F. et al. Enhancing oligodendrocyte myelination rescues synaptic loss and improves functional recovery after chronic hypoxia. *Neuron* **99**, 689–701 e685 (2018).
68. Funfschilling, U. et al. Glycolytic oligodendrocytes maintain myelin and long-term axonal integrity. *Nature* **485**, 517–521 (2012).
69. Lee, Y. et al. Oligodendroglia metabolically support axons and contribute to neurodegeneration. *Nature* **487**, 443–448 (2012).
70. Spitzer, S. O. et al. Oligodendrocyte progenitor cells become regionally diverse and heterogeneous with age. *Neuron* **101**, 459–471 e455 (2019).
71. Foerster, S., Hill, M. F. E. & Franklin, R. J. M. Diversity in the oligodendrocyte lineage: plasticity or heterogeneity? *Glia* **67**, 1797–1805 (2019).
72. Marques, S. et al. Transcriptional convergence of oligodendrocyte lineage progenitors during development. *Dev. Cell* **46**, 504–517 e507 (2018).
73. Marques, S. et al. Oligodendrocyte heterogeneity in the mouse juvenile and adult central nervous system. *Science* **352**, 1326–1329 (2016).
74. Yasuda, K. et al. Sex-specific differences in transcriptomic profiles and cellular characteristics of oligodendrocyte precursor cells. *Stem Cell Res.* **46**, 101866 (2020).
75. Trutzer, I. M., Garcia-Cabezas, M. A. & Zikopoulos, B. Postnatal development and maturation of layer 1 in the lateral prefrontal cortex and its disruption in autism. *Acta Neuropathol. Commun.* **7**, 40 (2019).
76. Zikopoulos, B. & Barbas, H. Changes in prefrontal axons may disrupt the network in autism. *J. Neurosci.* **30**, 14595–14609 (2010).
77. Galvez-Contreras, A. Y., Zarate-Lopez, D., Torres-Chavez, A. L. & Gonzalez-Perez, O. Role of oligodendrocytes and myelin in the pathophysiology of autism spectrum disorder. *Brain Sci.* **10**, https://doi.org/10.3390/brainsci10120951 (2020).
78. Khanbabaei, M. et al. Precocious myelination in a mouse model of autism. *Transl. Psychiatry* **9**, 251 (2019).

79. Havdahl, A. et al. Genetic contributions to autism spectrum disorder. *Psychol. Med.* **51**, 2260–2273 (2021).
80. Lasalle, J. M. Autism genes keep turning up chromatin. *OA Autism* **1**, 14 (2013).
81. Hoffmann, A. & Spengler, D. Chromatin remodeler CHD8 in autism and brain development. *J. Clin. Med.* **10**, https://doi.org/10.3390/jcm10020366 (2021).
82. Zhang, Z. et al. Autism-associated chromatin regulator Brg1/SmarcA4 is required for synapse development and myocyte enhancer factor 2-mediated synapse remodeling. *Mol. Cell. Biol.* **36**, 70–83 (2016).
83. Matuszek, G. & Talebizadeh, Z. Autism Genetic Database (AGD): a comprehensive database including autism susceptibility gene-CNVs integrated with known noncoding RNAs and fragile sites. *BMC Med. Genet.* **10**, 102 (2009).
84. Pinto, D. et al. Functional impact of global rare copy number variation in autism spectrum disorders. *Nature* **466**, 368–372 (2010).
85. De Rubeis, S. et al. Synaptic, transcriptional and chromatin genes disrupted in autism. *Nature* **515**, 209–215 (2014).
86. Zoghbi, H. Y. Postnatal neurodevelopmental disorders: meeting at the synapse? *Science* **302**, 826–830 (2003).
87. Penzes, P., Cahill, M. E., Jones, K. A., VanLeeuwen, J. E. & Woolfrey, K. M. Dendritic spine pathology in neuropsychiatric disorders. *Nat. Neurosci.* **14**, 285–293 (2011).
88. Noroozi, R. et al. Meta-analysis of GABRB3 gene polymorphisms and susceptibility to autism spectrum disorder. *J. Mol. Neurosci.* **65**, 432–437 (2018).
89. Silva, A. I. et al. Reciprocal white matter changes associated with copy number variation at 15q11.2 BP1-BP2: a diffusion tensor imaging study. *Biol. Psychiatry* **85**, 563–572 (2019).
90. Stefansson, H. et al. CNVs conferring risk of autism or schizophrenia affect cognition in controls. *Nature* **505**, 361–366 (2014).
91. Miles, J. H. Autism spectrum disorders—a genetics review. *Genet. Med.* **13**, 278–294 (2011).
92. Habermacher, C., Angulo, M. C. & Benamer, N. Glutamate versus GABA in neuron-oligodendroglia communication. *Glia* **67**, 2092–2106 (2019).
93. Braaker, P. N. et al. Activity-driven myelin sheath growth is mediated by mGluR5. *Nat. Neurosci.* **28**, 1213–1225 (2025).
94. Chen, T. J. et al. In vivo regulation of oligodendrocyte precursor cell proliferation and differentiation by the AMPA-receptor subunit GluA2. *Cell Rep.* **25**, 852–861.e857 (2018).
95. Hamilton, N. B. et al. Endogenous GABA controls oligodendrocyte lineage cell number, myelination, and CNS internode length. *Glia* **65**, 309–321 (2017).
96. Luyt, K. et al. Developing oligodendrocytes express functional GABA(B) receptors that stimulate cell proliferation and migration. *J. Neurochem.* **100**, 822–840 (2007).
97. van der Werf, I. M. et al. Behavioural characterization of AnkyrinG deficient mice, a model for ANK3 related disorders. *Behav. Brain Res.* **328**, 218–226 (2017).
98. Mohan, V. et al. Close homolog of L1 regulates dendritic spine density in the mouse cerebral cortex through semaphorin 3B. *J. Neurosci.* **39**, 6233–6250 (2019).
99. Guo, Y. et al. Elevated levels of FMRP-target MAP1B impair human and mouse neuronal development and mouse social behaviors via autophagy pathway. *Nat. Commun.* **14**, 3801 (2023).
100. Zeidan-Chulia, F. et al. Up-regulation of oligodendrocyte lineage markers in the cerebellum of autistic patients: evidence from network analysis of gene expression. *Mol. Neurobiol.* **53**, 4019–4025 (2016).
101. Kang, S. H., Fukaya, M., Yang, J. K., Rothstein, J. D. & Bergles, D. E. NG2+ CNS glial progenitors remain committed to the oligodendrocyte lineage in postnatal life and following neurodegeneration. *Neuron* **68**, 668–681 (2010).
102. Srinivas, S. et al. Cre reporter strains produced by targeted insertion of EYFP and ECFP into the ROSA26 locus. *BMC Dev. Biol.* **1**, 4 (2001).
103. Su, Y. et al. Astrocyte endfoot formation controls the termination of oligodendrocyte precursor cell perivascular migration during development. *Neuron* **111**, 190–201 e198 (2023).
104. Foo, L. C. Purification of rat and mouse astrocytes by immunopanning. *Cold Spring Harb. Protoc.* **2013**, 421–432 (2013).
105. Niu, J. et al. Aberrant oligodendroglial-vascular interactions disrupt the blood-brain barrier, triggering CNS inflammation. *Nat. Neurosci.* **22**, 709–718 (2019).
106. Wang, X., Su, Y., Hu, X. & Niu, J. Osmotic pump-based drug-delivery for in vivo remyelination research on the central nervous system. *J. Vis. Exp.* https://doi.org/10.3791/63343 (2021).
107. Ting, J. T. et al. Preparation of acute brain slices using an optimized n-methyl-D-glucamine protective recovery method. *J. Vis. Exp.* https://doi.org/10.3791/53825 (2018).
108. Liao, Y. et al. Spatial memory requires hypocretins to elevate medial entorhinal gamma oscillations. *Neuron* **112**, 155–173.e158 (2024).
109. Niu, J. et al. Connexin-based channels contribute to metabolic pathways in the oligodendroglial lineage. *J. Cell Sci.* **129**, 1902–1914 (2016).
110. dos Santos, Á et al. Autophagy receptor NDP52 alters DNA conformation to modulate RNA polymerase II transcription. *Nat. Commun.* **14**, 2855 (2023).
111. Bernstein, B. E., Humphrey, E. L., Liu, C. L. & Schreiber, S. L. The use of chromatin immunoprecipitation assays in genome-wide analyses of histone modifications. *Methods Enzymol.* **376**, 349–360 (2004).
112. Buck, M. J. & Lieb, J. D. ChIP-chip: considerations for the design, analysis, and application of genome-wide chromatin immunoprecipitation experiments. *Genomics* **83**, 349–360 (2004).
113. Schafer, D. P., Lehrman, E. K., Heller, C. T. & Stevens, B. An engulfment assay: a protocol to assess interactions between CNS phagocytes and neurons. *J. Vis. Exp.* https://doi.org/10.3791/51482 (2014).

Acknowledgements

This work was supported by grants from the National Key Research and Development Program of China (STI 2030—Major Projects, 2021ZD0201703 to J.N. and L.X.). National Natural Science Foundation of China (W2511095 and NSFC 32271034 to J.N.). Chongqing Natural Science Fund for Distinguished Young Scholars (CSTB 2023NSCQ-JQX0030 to J.N.). Chinese Natural Science Foundation (Institute of brain and intelligence, CNSF 31921003 to L.X.). Science Fund for Creative Research Groups of the Natural Science Foundation of Chongqing (cstc2019jcyj-cxttX0005, Q.Y.). We thank INTELLIPHECY for their assistance with the RNA-seq data analysis. We also would like to express our gratitude to Professor Chao He from the Department of Physiology at the Institute of Brain and Intelligence, Third Military Medical University, for his assistance with the electrophysiological experiments.

Author contributions

J.N. and L.X. conceived the study. J.N. designed the experiments. Xiaorui W., Z.W., Y. Shen, X.C., H.L., Y.Su., and J.N. performed the animal and cell culture experiments and analyzed the data. C.Z., Q.W., and Xiaorui W. performed analysis of the RNA-seq data. Xiaorui W., M.L., Xiao W., Y.X., and S.W. performed the electrophysiological experiments and analyzed the data. A.V., C.Y., H.C., C.H., N.S., W.M., and Q.Y. contributed to the discussion. J.N. and Xiaorui W. wrote the manuscript. A.V., C.Y., H.C., and L.X. made the editing. J.N. is the lead contact.

Competing interests
The authors declare no competing interests.

Additional information
Supplementary information The online version contains supplementary material available at https://doi.org/10.1038/s41467-025-67930-y.

Correspondence and requests for materials should be addressed to Jianqin Niu or Lan Xiao.

Peer review information *Nature Communications* thanks Lucas Cheadle and the other, anonymous, reviewers for their contribution to the peer review of this work. A peer review file is available.

[1]Department of Histology and Embryology, Chongqing Key Laboratory of Neurobiology, Third Military Medical University, Chongqing, China. [2]Biomedical Analysis Research Centre, Third Military Medical University, Chongqing, China. [3]Department of Physiology, Institute of Brain and Intelligence, Third Military Medical University, Chongqing, China. [4]Department of Neurobiology, School of Basic Medical Sciences; Key Laboratory of Major Brain Disease and Aging Research (Ministry of Education), Chongqing Medical University, Chongqing, China. [5]Seventh Affiliated Hospital of Sun Yat-sen University, Shenzhen, China. [6]Department of Neurobiology, Third Military Medical University, Chongqing, China. [7]School of Life Sciences, Faculty of Science, University of Technology Sydney, Ultimo, NSW, Australia. [8]State Key Laboratory of Genetic Resources and Evolution, Key Laboratory of Animal Models and Human Disease Mechanisms of Yunnan Province, Kunming Institute of Zoology, Chinese Academy of Sciences, Kunming, China. [9]Sir Run Run Shaw Hospital, Department of Immunology, School of Basic Medical Science, Zhejiang University, Hangzhou, China. [10]Liangzhu Laboratory, Hangzhou, China. [11]Department of Neurology, Second Affiliated Hospital, Chongqing Institute for Brain and Intelligence, Third Military Medical University, Chongqing, China. [12]Faculty of Biology, Medicine and Health, The University of Manchester, Manchester, UK. [13]Department of Neurosciences, University of the Basque Country, Leioa, Spain. [14]IKERBASQUE Basque Foundation for Science, Bilbao, Spain. [15]Department of Stem Cell Biology, State Research Institute, Centre for Innovative Medicine, Vilnius, Lithuania. [16]Department of Forensic Analytical Toxicology, School of Forensic Medicine, China Medical University, Shenyang, China. [17]Key Laboratory of Major Brain Disease and Aging Research, Chongqing Medical University, Chongqing, China. [18]State Key Laboratory of Trauma and Chemical Poisoning, Chongqing, China. [19]Department of Neurosurgery, Second Affiliated Hospital, Third Military Medical University, Chongqing, China.
✉e-mail: jianqinniu@tmmu.edu.cn; xiaolan35@hotmail.com